Ludwig-Maximilians-Universität München
Sektion Physik

Bestimmung der Masse des W-Bosons aus der direkten Rekonstruktion semileptonischer W-Paar-Zerfälle

Diplomarbeit

von

Birgit Bußmann

August 2001

Erstgutachterin: Prof. Dr. Dorothee Schaile
Zweitgutachter: Prof. Dr. Martin Faessler

Ludwig-Maximilians-Universität München
Sektion Physik

Determination of the W Boson Mass in the Semileptonic Event Topology

Diplomarbeit

von

Birgit Bußmann

August 2001

A mind once stretched by a new idea
never regains its original dimensions.
Anonymous

Abstract

This analysis deals with the measurement of the mass of the W boson in the semileptonic channel. It employs a method developed in [1] for the analysis of data at $\sqrt{s} = 183\,GeV$ and $\sqrt{s} = 189\,GeV$. This method is based on a special unbinned likelihood fit to the invariant mass spectra of the W boson, referred to as convolution fit. It takes into account the asymmetric measurement errors of each individual event, an information, which is lost in the standard fit of an analytical function to the measured spectra. This diploma thesis extends this method to data at center-of-mass energies between 192 and 206.5 GeV. Systematic studies are made for each center-of-mass energy. Furthermore, the use of Lagrange multipliers in the calculation of the event probability density is investigated but shows less stable results.

The analysis of data with a total integrated luminosity of 437.6 pb^{-1} yields a measured W boson mass of

$$M_W = 80.575 \pm 0.079 \pm 0.052\,GeV$$

This result is consistent with the results of other direct measurements including a preliminary OPAL result for the mass of the W boson in the semileptonic channel. It is also in agreement with an indirect determination of the W boson mass based on the size of radiative corrections to precise electroweak measurements of fermion pair production in e^+e^--collisions.

Contents

List of Figures

List of Tables

Introduction

Elementary particles — the constituents of matter. What are they really like?

In contrast to other fields of physical research, particle physics enters regions, where the observation of physical objects and their interactions becomes harder and harder. The times when physics was restricted to the analysis of the laws of gravitation or classical mechanics have long passed. Modern physics confronts us with topics that make research both more complicated and more fascinating than it ever was before. Everyday life, of course, is dominated by classical mechanics, reaching out to relativistic mechanics for all processes implying higher speed and to quantum mechanics when the analyzed objects are reduced in size. Both aspects are given in particle physics.

It was not until the seventies of the 20th century that the established physical theories — with the exception of gravitation — were combined to a new theory. The so called *Standard Model* was designed to describe elementary particles and their interactions and has met the expectations of modern physics until this very day. In this theory, all fundamental interactions are derived from a single principle, the local gauge invariance. Interactions between particles are seen as the exchange of a so called *gauge boson*. The Z^0 and the $W^{\pm}$ bosons are such gauge bosons.

They were discovered at the CERN research center in 1983. The CERN is an international collaboration of 20 member states worldwide, including Germany. It is located just outside the city of Geneva in Switzerland. The last 12 years mark the LEP era. At the **L**arge **E**lectron **P**ositron collider, particles were produced in electron-positron collisions and detected at the 4 experiments: ALEPH, DELPHI, OPAL and L3. LEP1 started operation in 1989. Until 1995, millions of events were accumulated. The most important achievements during this period were high precision measurements of the properties of the Z^0 boson. After that, LEP1 was upgraded to higher energy regions. The LEP2 era started in 1996. The new energy regions exceeding 161 GeV now provided the collaboration with the means to produce and analyze W^+W^- pairs. In 2000, the days of LEP2 were counted as well. Data taking finally ended at the OPAL detector on the 2nd of November. But the analysis of data collected in the last years still goes on.

The determination of the W boson mass from W boson pair decays in the semileptonic channel will be the topic of this analysis. The convolution method is applied to data events collected at the OPAL detector in 1999 and 2000 including center-of-mass energies between 192 and 206.5 GeV.

Chapter 1

Theoretical Background Part I: The Standard Model

Modern particle physics is generally described by the so called *Standard Model*, a gauge theory based on $SU(3)_c \otimes SU(2)_L \otimes U(1)_Y$ symmetry. This theory contains a number of fundamental particles that can roughly be divided into two groups: Spin 1/2 particles known as *fermions* and Spin 1 particles known as *bosons*. Whereas fermions are the particles matter is built of, bosons are responsible for interactions of matter. Interactions between fundamental particles are seen as the exchange of gauge bosons between the constituents of matter. These gauge bosons are massless photons to mediate the electromagnetic force, massive Z^0 and W^+/W^- bosons to mediate the weak force and gluons to mediate the strong force. In addition to that, the Standard Model introduces a spin 0 particle, the Higgs boson[1]. The existence of the Higgs boson is the consequence of a mechanism called *spontaneous symmetry breaking* that is needed to give mass to the particles included in the Standard Model. The fundamental particles and their interactions will be described in further detail in the following sections.

1.1 Elementary Constituents of Matter

According to the Standard Model all matter is built of 12 fundamental[2] fermions, six leptons and six quarks. Quarks are the only fundamental fermions that are subject to the strong force. They occur in three different *colours*. The other fundamental fermions are known as leptons: electron, muon and tau leptons. All these particles are further classified. They are assigned to three different *generations*, each of which contains two quarks and two leptons along with the corresponding antiparticles. The first generation includes the electron (e), the electron neutrino (ν_e), the up quark (u) and the down quark (d). The muon (μ), the muon neutrino (ν_μ), the charm quark (c) and the strange quark (s) belong to the second generation. And finally there is the third generation consisting of the tau lepton (τ), the tau neutrino (ν_τ), the top quark (t) and the bottom quark (b). Stable matter is almost entirely built of members of the first generation. The particle masses

[1] Unfortunately the Higgs boson has not yet been observed directly.

[2] Apparently without inner structure.

increase with each generation.

1.2 Fundamental Interactions

As far as we know today, there are only four fundamental forces at work in nature: *strong, electromagnetic, weak* and *gravitational* interaction. The following table shows them in order of decreasing strength:

force	strength	theory	exchanged particle
strong	10^{1}	Quantum Chromo Dynamics	gluon
electromagnetic	10^{-2}	Quantum Electro Dynamics	photon
weak	10^{-13}	Flavour Dynamics	$W^+/W^-, Z^0$
gravitational	10^{-42}	Geometro Dynamics	(graviton[3])

Table 1.1: *Fundamental forces*

Even though attempts have been made to include gravitation into the theory of particle physics it is not included in the Standard Model[4]. But gravitation is — compared to the strong, the electromagnetic and the weak force — negligible when it comes to particle physics and energy scales reached by the LEP collider. For this analysis, two forces and their corresonding theories must be discussed in further detail: the *weak* and the *electromagnetic force*. And, of course, the unification of both theories, the *electroweak unification*.

1.2.1 The Electromagnetic Force

Quantum Electro Dynamics (QED), the theory describing the electromagnetic force, is the most basic result of the gauge principle. The existence of the gauge boson of QED, the photon, is a direct consequence of this principle. Gauge bosons and their properties can generally be deduced from the postulated local gauge invariance and the symmetry groups of the underlaying particles. The so called *local gauge transformation* is a unitary[5] transformation of the following form:

$$\psi \rightarrow \psi' = U\psi = e^{i \sum_{\alpha=1}^{N^2-1} \theta_\alpha(x) T_\alpha} \psi \tag{1.1}$$

We consider a symmetry group of the dimension N. T_α denotes the generator of the symmetry group, ψ the fields of the particles and θ_α is an arbitrary transformation parameter depending on time and space. Considering only QED there is but one generator, the electromagnetic charge q. Equation (1.1) therefore changes to

[3] This particle has not yet been observed.

[4] In contrast to the theories describing strong, electromagnetic and weak forces, the theory describing gravitation is not gauge invariant.

[5] $UU^\dagger = 1$

$$\psi \rightarrow \psi' = U\psi = e^{i\theta(x)q}\psi \ . \tag{1.2}$$

The principle of local gauge invariance asks for invariance of the equations of motion with regard to these transformations U. As the equations of motion can be deduced by derivating the Lagrangian, it should be subject to the local gauge invariance itself. The Lagrangian for fermions is given by

$$\mathcal{L} = i\bar{\psi}\gamma^{\mu}\partial_{\mu}\psi - m\bar{\psi}\psi \ . \tag{1.3}$$

In this equation, γ^{μ} denote the Dirac matrices and m the mass of the electron. The Lagrangian as given above is invariant under global[6] transformations. But when it comes to local transformations one has to consider an additional phase factor changing in space[7]. Derivating the Lagrangian therefore yields an additional factor $\partial_{\mu}U$. To insure invariance nevertheless we have to introduce the so called *covariant derivative*,

$$D_{\mu} = \partial_{\mu} - iqA_{\mu} \ , \tag{1.4}$$

along with a new vector field A_{μ}. Again, q denotes the electromagnetic charge. For infinitesimal transformations U local invariance is given in combination with a simultaneous transformation of the vector field A_{μ},

$$A'_{\mu} = A_{\mu} + \partial_{\mu}\theta(x) \ . \tag{1.5}$$

The following equation, the *Dirac equation*

$$(i\gamma^{\mu}D_{\mu} - m)\psi(x) = 0 \ , \tag{1.6}$$

is thus left unchanged. Now we have to consider another equation describing a vector field, the *Proca equation*. It describes a particle with spin 1 and mass M and is given by

$$\partial_{\mu}F^{\mu\nu} + M^2A^{\nu} = 0 \ , \tag{1.7}$$

with $F^{\mu\nu} = \partial^{\mu}A^{\nu} - \partial^{\nu}A^{\mu}$. The Proca equation (1.7) is only invariant if M is equal to zero. Equation (1.7) thus yields the Maxwell equations in vacuum well known from classical electrodynamics. We obtain a massless gauge boson of infinite interaction range, the photon.

[6] U(x) is constant respectively θ=const.
[7] $\theta = \theta(x)$

1.2.2 The Weak Force

When handling QED alone it is enough to consider abelian[8] groups. But for the other theories included in the Standard Model the concept of gauge invariance has to be further enlarged considering non-abelian groups as well. We might for instance look at the interaction between a lepton and its corresponding neutrino. When the lepton is changed into a neutrino, both particles must be arranged in a *doublet*. All particles taking part in weak interaction are arranged in doublets of the weak isospin. The resulting wave function is given by a product of the wave function of the lepton $\psi_l(x)$ and the isospinor χ and can be written in a form we already know from chapter 1.2.1, equation (1.1),

$$\psi' = e^{\frac{i}{2}\vec{\tau}\vec{\alpha}(x)}\psi \ , \tag{1.8}$$

where $\vec{\tau} = (\tau_1, \tau_2, \tau_3)$ are the Pauli matrices and $\vec{\alpha}$ is the vector of the three rotation angles. This transformation is identical to a rotation of the weak isospin in two dimensions and therefore belongs to the SU(2) group, the group of special[9] unitary matrices in 2 dimensions. Following the example of QED three external vector fields W_1^α, W_2^α and W_3^α are introduced to insure invariance with regard to local gauge transformations. When analysing SU(N) groups in general we obtain the following equation for infinitesimal transformations of gauge fields F_μ^α:

$$\mathrm{F'}_\mu^\alpha = F_\mu^\alpha - \frac{1}{g}\partial_\mu\theta^a + f_{\alpha\beta\gamma}F_\mu^\beta\theta^\gamma \tag{1.9}$$

where g denotes the coupling constant of the corresponding symmetry group respectively the interaction. $f_{\alpha\beta\gamma}$ is given by $[T_\alpha, T_\beta] = if_{\alpha\beta\gamma}T^\gamma$ and in the special case of the SU(2) symmetry group of weak interaction $f_{\alpha\beta\gamma}$ equals the total antisymmetric tensor $\epsilon_{\alpha\beta\gamma}$.

1.2.3 The Electroweak Unification

The QED and the weak force alone do not account for all aspects of the behaviour of observed particles. There are certain effects that call for a combined treatment of the electromagnetic and the weak force, first of all the fact that the weak interaction is parity violating. Particles subject to the weak force can change their identity emitting a weak field quantum as multiplets of the weak isospin I. Experimental evidence shows that charged weak currents only couple to left handed fermions. They are therefore arranged in doublets, while right handed leptons are arranged in singlets. The left handed fermions respectively the right handed antifermions built doublets of the weak isospin $I = \frac{1}{2}$. The right handed charged leptons and quarks respectively the left handed antileptons and antiquarks do not couple to the charged weak field quantum, the $W^\pm$ boson, they built singlets of the weak isospin 0. All fundamental fermions are listed below (table 1.2) along with the weak isospin.

[8] $[T_\alpha, T_\beta] = 0$

[9] det U=0

leptons			I	I_3
$\begin{pmatrix} \nu_e \\ e^- \end{pmatrix}_L$	$\begin{pmatrix} \nu_\mu \\ \mu^- \end{pmatrix}_L$	$\begin{pmatrix} \nu_\tau \\ \tau^- \end{pmatrix}_L$	$\frac{1}{2}$ $\frac{1}{2}$	$\frac{1}{2}$ $-\frac{1}{2}$
e^-_R	μ^-_R	τ^-_R	0	0

quarks			I	I_3
$\begin{pmatrix} u \\ d' \end{pmatrix}_L$	$\begin{pmatrix} c \\ s' \end{pmatrix}_L$	$\begin{pmatrix} t \\ b' \end{pmatrix}_L$	$\frac{1}{2}$ $\frac{1}{2}$	$\frac{1}{2}$ $-\frac{1}{2}$
u_R d'_R	c_R s'_R	t_R b'_R	0 0	0 0

Table 1.2: *Fundamental fermions and the weak isospin. I_3 denotes the third component of the weak isospin.*

The weak force couples to the following doublets

$$\begin{pmatrix} u \\ d' \end{pmatrix}, \begin{pmatrix} c \\ s' \end{pmatrix}, \begin{pmatrix} t \\ b' \end{pmatrix} \tag{1.10}$$

instead of the usual quark doublets

$$\begin{pmatrix} u \\ d \end{pmatrix}, \begin{pmatrix} c \\ s \end{pmatrix}, \begin{pmatrix} t \\ b \end{pmatrix} \tag{1.11}$$

wherein d', s' and b' are linear combinations of the physical quarks d, s and b. Their mixing ratio is given by the *Cabbibo-Kobayashi-Maskawa-Matrix* [4].

A simple $U(1)_{em} \otimes SU(2)_{weak}$ treatment is not enough to describe the behaviour of the particles properly. A unified theory based on $SU(2)_L \otimes U(1)_Y$ symmetry has been introduced by **G**lashow, **S**alam and **W**einberg along with a new variable Y, the *hypercharge*. The GSW theory takes the fact into account that fermions are arranged in left handed doublets and right handed singlets: The $SU(2)_L$ part couples to left handed fermions whereas the $U(1)_Y$ part couples to both right and left handed fermions. The electromagnetic charge Q_{em} is given by the *Gell-Mann-Nishijima relation*

$$Q_{em} = I_3 + \frac{1}{2}Y \ . \tag{1.12}$$

$SU(2)_L \otimes U(1)_Y$ symmetry requires the existence of four spin 1 vector fields. A triplet $W_\mu^{1,2,3}$ is introduced for the $SU(2)_L$ part and a singlet B_μ is added to ensure $U(1)_Y$

symmetry. Linear combinations of these vector fields yield the actual physical fields now given by

$$A_\mu = B_\mu cos(\theta_W) + W^3_\mu sin(\theta_W) \ , \tag{1.13}$$

$$Z_\mu = -B_\mu sin(\theta_W) + W^3_\mu cos(\theta_W) \ , \tag{1.14}$$

$$W^\pm_\mu = \frac{1}{\sqrt{2}}(W^1_\mu \mp W^2_\mu) \ , \tag{1.15}$$

where θ_W denotes the electroweak mixing angle. At this point the theory confronts another problem: All these vector bosons are massless. One could therefore exspect an infinite range of the weak interaction. This proves to be a clear contradiction to experimental results: the weak interaction has a range of about 10^{-13} m. This problem is solved by a mechanism known as *spontaneous symmetry breaking*. A SU(2) doublet of complex scalar Higgs fields with a non-vanishing expectation value is introduced:

$$\Phi = \begin{pmatrix} \Phi^+ \\ \Phi^0 \end{pmatrix} \tag{1.16}$$

The Higgs field couples to the electroweak gauge bosons, giving mass and thus finite range to the three weak gauge bosons while leaving the electromagnetic part of the theory, the $U(1)_{em}$ symmetry, unbroken. The potential describing self interaction of the Higgs field is given by

$$V(\Phi) = -\mu^2 \Phi^\dagger \Phi + \frac{\lambda}{4}(\Phi^\dagger \Phi)^2 \tag{1.17}$$

with the free parameters μ and λ and a vacuum expectation value of Φ of $\nu = \frac{2\mu}{\lambda}$. Using the freedom of gauge transformation and selecting a suitable ground state of the Higgs doublet it is now possible to make three of the four Higgs fields disappear. Their degrees of freedom are absorbed in the vector fields of the — now massive — gauge bosons. The remaining component of the Higgs doublet becomes the massive neutral Higgs boson included in the Standard Model. The resulting masses of the gauge bosons are given by

$$M_Z = \frac{1}{2}\sqrt{g_1^2 + g_2^2}\,\nu \tag{1.18}$$

$$M_W = \frac{1}{2} g_2 \,\nu \tag{1.19}$$

whereas the mass of the photon — the $SU(2)_{em}$ symmetry being unbroken — remains zero. g_1 and g_2 are the coupling constants of the corresponding symmetry groups $U(1)_Y$ and $SU(2)_L$. The electroweak mixing angle is also defined by the gauge coupling constants g_1 and g_2. Is is given by

$$cos(\Theta_W) = \frac{g_2}{\sqrt{g_1^2 + g_2^2}} \tag{1.20}$$

Equations (1.18) and (1.19) show that the electroweak mixing angle can be determined by measuring the masses of the charged gauge boson $W^{\pm}$ and the neutral Z^0 boson as the mixing angle can also be expressed as the ratio of the corresponding masses:

$$cos(\Theta_W) = \frac{M_W}{M_Z} \tag{1.21}$$

The gauge coupling constants themself can be determined by using the following relations for the electromagnetic charge e and the mass of the W boson M_W:

$$e = \frac{g_1 g_2}{\sqrt{g_1^2 + g_2^2}} \tag{1.22}$$

$$M_W = \sqrt{\frac{\pi\alpha}{\sqrt{2}G_F}} \frac{1}{sin(\Theta_W)} \tag{1.23}$$

where G_F denotes the Fermi constant and α the fine structure constant. The mass of the Higgs boson is given by $M_H = \sqrt{2}\,\mu$.

1.2.4 The Strong Force

In analogy to the theories explained above, especially the QED, the theory of strong interaction, *Quantum Chromo Dynamics (QCD)*, is formulated as a gauge theory as well. QCD is based on SU(3) colour symmetry and describes the strong interaction between quarks. In constrast to the QED, where only one massless neutral gauge boson is needed, the QCD introduces eight massless gauge bosons, the gluons. There are three different *colours* commonly referred to as red, green and blue and their correspondending anticolours. As the gluons themself carry colour charge, they are able to interact with one another. There is another special aspect of the QCD that calls for further explanation: the *running* of the coupling constant α_s. While α_s and thus the resulting force gets smaller for distances in dimensions that are small compared to the size of a proton or a pion — a phenomenon commonly known as *asymptotic freedom* — it increases with growing distances between the quarks. Quarks can therefore move within these particles without interaction. The running of α_s also accounts for the fact that single quarks have not yet been observed: The energy density between two colour charges being separated from one another soon becomes large enough to create quark-antiquark pairs or gluons leading to the *fragmentation* of the original particles. As a consequence of this fragmentation there are no isolated quarks carrying colour charge. This behaviour is called *confinement*. Observed hadrons must thus consist of corresponding quark-antiquark pairs (mesons) or of three quarks of different colours (baryons) complementing one another to colour neutral or *white*.

Chapter 2

Theoretical Background Part II: W Boson Pairs

W boson pairs can be observed in e^+e^--collisions as soon as the center-of-mass energy reaches a limit of about two times the mass of a single W boson. As energies available at LEP2[1] are well beyond that limit, W boson pair physics is certainly worth a closer look. In the following chapter, a short introduction on the W boson mass in general is given and four- and two-fermion processes are presented. The chapter closes with a description of the three different decay channels of W boson pairs.

2.1 The Mass of the W Boson

As already mentioned in chapter 1.2.3, the mass of the W Boson is given by

$$M_W = M_Z \, cos(\theta_W) = \sqrt{\frac{\pi\alpha}{\sqrt{2}G_F}} \frac{1}{sin(\Theta_W)} \tag{2.1}$$

where G_F denotes the Fermi constant, α the fine structure constant and θ_W the electroweak mixing angle. Equation (2.1) determines the mass at tree level (lowest order perturbation theory). It shows that the W boson mass can be determined indirectly by measuring other Standard Model parameters. Global fits to all data obtained from LEP2 and the $p\bar{p}$ collider — except direct measurement of M_W — yield a mass of $80.368 \pm 0.023\, GeV$ [5]. For higher order perturbations, the mass of the W boson also depends on the masses of the top quark and the Higgs boson. Including one loop corrections — as shown in figure 2.1 — the mass of the W boson amounts to

$${M_W}^2 = \frac{\pi\alpha}{\sqrt{2}G_F \, sin^2(\Theta_W)} \left(1 + \frac{3G_F}{8\pi^2\sqrt{2}} M_t^2 + \frac{2G_F}{16\pi^2} M_W^2 \left(\frac{11}{3} \ln \frac{M_H^2}{M_W^2} + \ldots\right)\right) \tag{2.2}$$

where M_H denotes the mass of the Higgs boson and M_t the mass of the top quark [2].

[1] see chapter 4

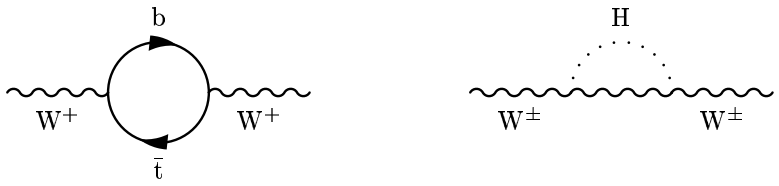

Figure 2.1: *One-loop corrections to the W propagator*

Direct measurements of the W boson mass — especially high precision measurements — can thus be seen as a cross-check on the Standard Model itself. They furthermore allow the estimation of a Higgs mass, as the Higgs boson itself has not yet been detected.

2.2 Pair Production of W Bosons

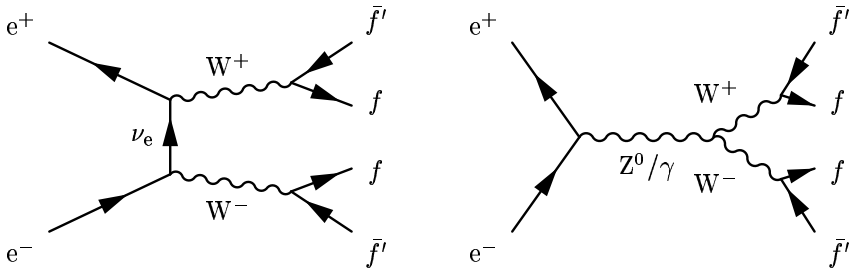

Figure 2.2: *Lowest order Feynman diagrams describing the production of W boson pairs in e^+e^--collisions: neutrino exchange (left) and e^+e^--annihilation (right)*

Pair production of W bosons in e^+e^--collisions can be observed as soon as the center-of-mass energy exceeds an energy threshold of about two times the mass of the W boson. This threshold is reached at about 161 GeV. At tree level, only the lowest order Feynman diagrams contribute to the production of W boson pairs: the t-channel diagram mediated by neutrino exchange and the s-channel diagrams mediated by Z^0 and γ. They are depicted in figure 2.2. These fundamental Feynman diagrams are referred to as CC03 Feynman diagrams. At energies close to the energy threshold of 161 GeV the cross section is dominated by neutrino exchange (t-channel diagram).

W boson mass distributions are described by relativistic Breit-Wigner functions $\rho(x)$

$$\rho(x) = \frac{1}{\pi}\frac{\Gamma_W}{M_W}\frac{x}{(x - M_W^2)^2 + x^2(\frac{\Gamma_W}{M_W})^2} \tag{2.3}$$

where $\sqrt{x}$ denotes the mass of the W boson. M_W is the pole mass and Γ_W the width of the W boson. To calculate *on-shell* Born-level[2] cross sections, the W bosons are considered as stable, yielding the cross section σ_0. It can be written in terms of the ν_e, γ and Z^0 exchange contributions and their interferences [7]: The quadratic sum of the amplitudes associated with the CCO3 diagrams yields σ_0. The total *off-shell* Born-level cross section is given by a convolution of the on-shell cross section σ_0 with the different mass distributions $\rho(x_1)$ and $\rho(x_2)$ representing the two W bosons.

$$\sigma(s) = \int_0^s dx_1 \int_0^{(\sqrt{s}-\sqrt{x_1})^2} dx_2 \rho(x_1)\rho(x_2)\sigma_0(s, x_1, x_2) \tag{2.4}$$

with a center-of-mass energy of $\sqrt{s}$. Now further corrections are applied to compensate for radiative effects: Initial State Radiation (ISR) — the emission of a photon by the electron or positron before the collision point is reached — and the Coulomb singularity — the exchange of low energy photons between the W bosons. The total cross section of the W boson pair production as a function of the center-of-mass energy is depicted in figure 2.3.

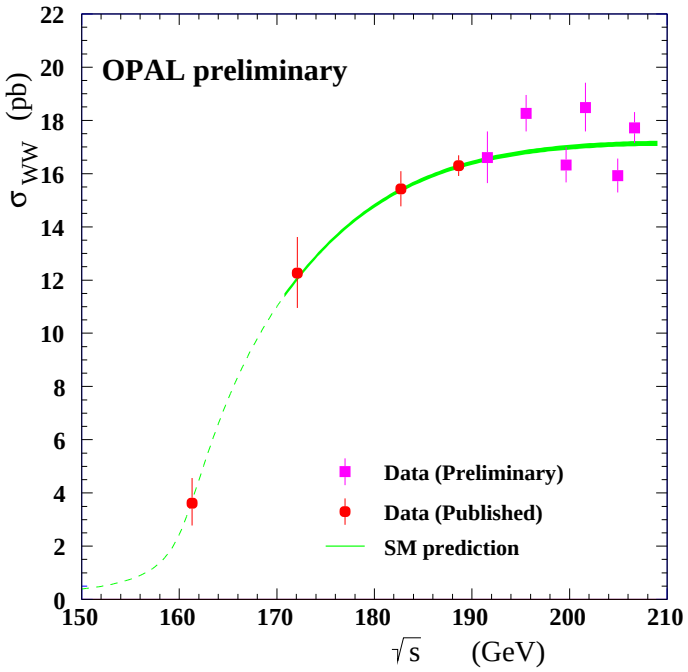

Figure 2.3: *The total cross section of W boson pair production as a function of the center-of-mass energy as measured by OPAL at* $\sqrt{s} = 161 - 207\,GeV$. *The solid band shows the Standard Model expectations obtained from Monte Carlo studies [6].*

[2] lowest order calculation

2.3 Four Fermion Processes in General

The contribution of the CCO3 diagrams to the cross section of W boson pair production has already been described in chapter 2.2. But when it comes to four-fermion processes in general one also has to consider the influence of other processes. They originate from e^+e^--collisions and end in four-fermion final states as well but pass different intermediate states. Four-fermion processes in general can be described by a set of six fundamental Feynman diagrams (depicted in figures 2.4 and 2.5). They are subdivided into abelian and non-abelian diagrams: diagrams lacking and diagrams including triple gauge boson vertices. The CCO3 Feynman diagrams can be classified accordingly: Neutrino exchange belongs to the group of abelian diagrams, the production of W boson pairs via e^+e^-- annihilation to the group of non-abelian diagrams.

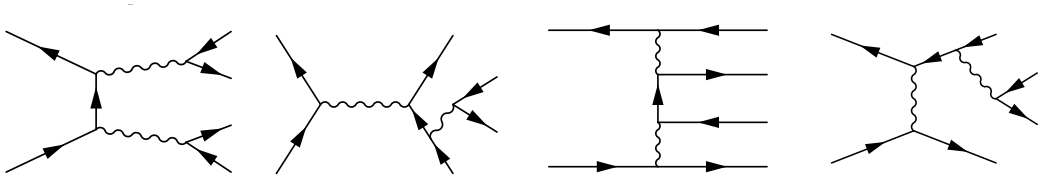

Figure 2.4: *Schematic view of abelian four-fermion diagrams. Straight lines: fermions. Wavy lines: gauge bosons:* W^+, W^-, γ *or* Z^0

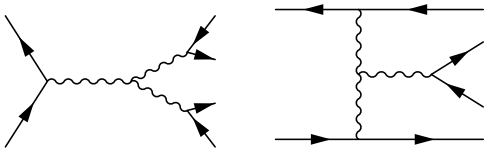

Figure 2.5: *Schematic view of non-abelian four-fermion diagrams. Straight lines: fermions. Wavy lines: gauge bosons. Two of the three wavy lines in each diagram mark W bosons*

Interference effects between Feynman diagrams describing W boson pair production and diagrams with equal final states have to be taken into account when measuring the mass of the W boson. Still, these effects are considered small enough to separate the cross section of four-fermion effects roughly into 'signal' and 'background' contributions. The 'signal' part contains all processes of W boson pair production.

$$\sigma_{4f} = \sigma_{WW} + \sigma_{bg} \tag{2.5}$$

The W^+W^- part (signal part) can be written as

$$\sigma_{WW} = \sigma_0^{WW}(1 + \delta_{EW} + \delta_{QCD}) \tag{2.6}$$

where the various terms correspond to

- σ_0^{WW}: the Born contribution from CC03 Feynman diagrams
- δ_{EW}: the electroweak radiative corrections
- δ_{QCD}: the QCD corrections to W^+W^- final states

The 'background' part of the total cross section consists of several non-WW four-fermion processes. The lowest order Feynman diagrams of background processes with four-fermion final states are depicted in figure 2.3, showing (from left to right): annihilation, Bremsstrahlung, two diagrams of conversion processes and fusion.

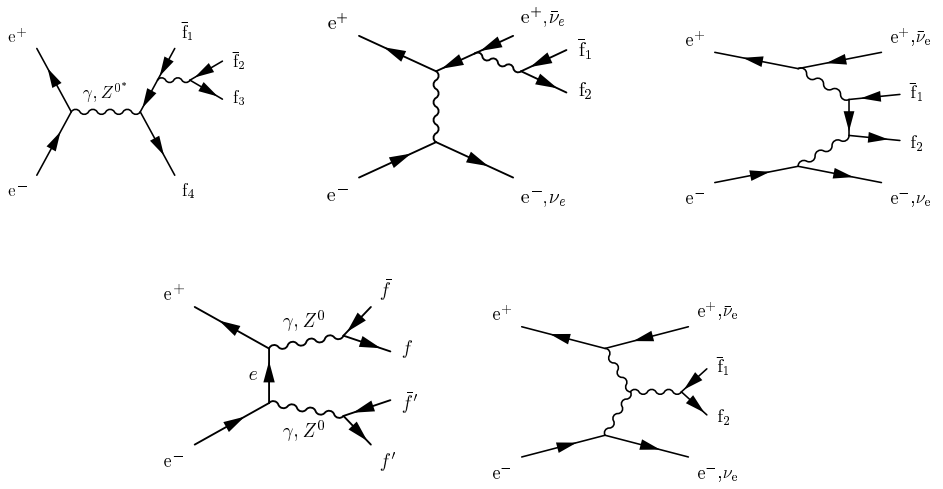

Figure 2.6: *Lowest order Feynman diagrams describing four-fermion non-WW processes*

The most important four-fermion background processes that have to be considered in the measurement of the W boson mass in the the semileptonic channel are the production of single W bosons ($We\nu$) and Z^0 pairs (ZZ).

2.4 Two Fermion Processes

Another background to W boson pair physics has to be taken into account, a background belonging to the class of two-fermion processes: the decay of Z^0/γ into $q\bar{q}$ ($e^+e^- \to Z^0/\gamma \to q\bar{q}$). Feynman diagrams describing two-fermion processes are shown in figure 2.7.

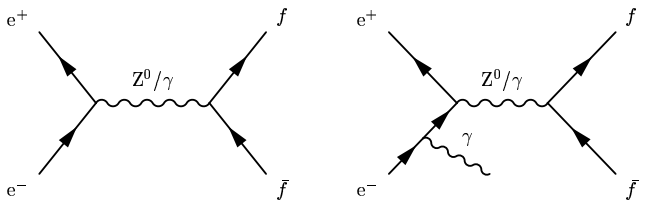

Figure 2.7: *Feynman diagrams describing two fermion processes*

Initial State Radiation plays an important role when dealing with this sort of background processes. LEP2 runs at considerably high energies exceeding the Z^0 resonance peak by far. But the emission of a photon by an incoming electron or positron lowers the center-of-mass energy to regions favouring the production of single Z^0 and thus enhances the cross section of two-fermion processes notably. The extent of this enhancement can be seen in figure 2.8: $\Sigma\, q\bar{q}\,(ISR)$ marks the cross section for $e^+e^- \to Z^0/\gamma \to q\bar{q}$ background, Initial State Radiation is taken into account. $\Sigma q\bar{q}$ denoted the cross section for the same process lacking this correction. Along with the cross section for two-fermion effects, the graphic depicts different cross sections for four-fermion effects as well, especially the cross section for W boson pair production denoted by WW.

2.5 Decay of W Boson Pairs

The decay channels of W boson pairs can be classified as fully hadronic, fully leptonic and — most important for this analysis — semileptonic.

In the *fully hadronic* channel, both W bosons decay into quark-antiquark pairs:

$$W^+W^- \to q\bar{q}q\bar{q}$$

Practically all energy is converted into hadrons, one expects at least four jets. Due to gluon emission by primary quarks, five and more jets can be observed. The recombination of those jets can be rather difficult as it is possible to combine four jets in three different ways to yield the original W bosons. A wrong jet recombination yields an additional background in the fully hadronic channel, the so called *combinatorial background*. The main advantages of the hadronic channel are high statistics — 45 percent of all W boson pairs decay hadronically — and the fact that a complete reconstruction of the event is possible as no energy is carried away by undetected neutrinos. On the other hand there is combinatorial background in this channel that does not exist in the other channels and

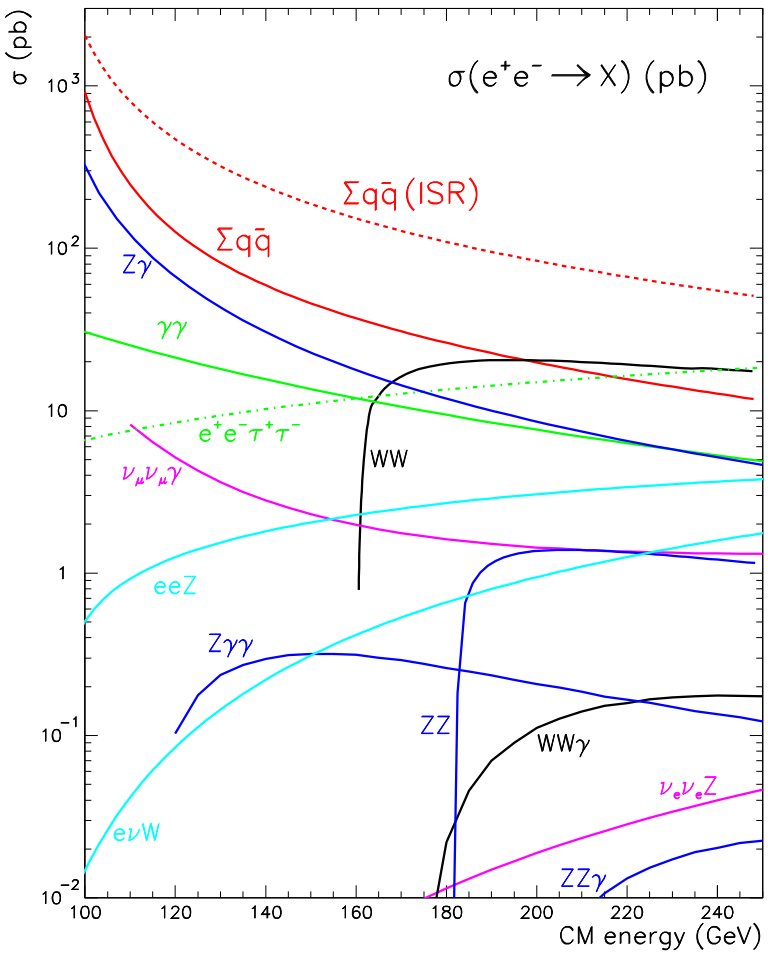

Figure 2.8: *Cross sections for important two- and four-fermion processes within the energy range of LEP2. WW marks the cross section of W boson pair production and* $\Sigma q\bar{q}$ *respectively* $\Sigma q\bar{q}(ISR)$ *the cross section of two-fermion processes. Important background from four-fermion processes is also included, marked as* $e\nu W$ *(single W production),* eeZ *(single* Z^0 *production) and* ZZ *(*Z^0 *pair production)*

Final State Interactions — Bose-Einstein Correlations [8] and Colour Reconnection [9] — further complicate the reconstruction of the mass of the W boson.

In the *fully leptonic* channel, both W bosons decay into lepton-neutrino pairs:

$$W^+W^- \rightarrow \bar{l}\nu l\bar{\nu}$$

Leptonic decays of W boson pairs are characterized by two energetic leptons and a large amount of missing energy carried away by undetected neutrinos. Narrow hadronic low multiplicity jets can be observed as well if one (or both) of the leptons happens to

be a hadronically decaying tau lepton. The fully leptonic channel is the channel with the clearest signature in the detector: Two energetic leptons or low multiplicity jets. There is no combinatorial background and there are no effects of Final State Interaction that complicate the event reconstruction in the fully hadronic channel. But the two unobserved neutrinos escape with an unknown amount of energy, making the complete event reconstruction impossible. In addition to that only 11 percent of all W boson pairs decay leptonically, the statistics of this channel are therefore comparatively low.

Last but not least there is the *semileptonic* channel where the W boson pair decays into a quark-antiquark and a lepton-neutrino pair:

$$W^+W^- \rightarrow \mathrm{q\bar{q}}l\bar{\nu}$$

In the semileptonic channel, one expects the detection of two hadronic jets and a single lepton or — if the leptonic part of the W boson pair decay consists of a tau-neutrino pair — a low multiplicity jet originating from subsequent tau decay. Due to the undetected neutrino there will also be missing energy. As there is only one lepton-neutrino pair in the semileptonic channel it is possible to fully reconstruct the event using the equations of constraint, the conservation of energy and momentum. The kinematic reconstruction is less constraint and thus less exact that the reconstruction in the fully hadronic channel, but on the other hand there is no combinatorial background and no Final State Interaction that complicates the event reconstruction in the hadronic channel. The statistics of the semileptonic channel are comparable to the statistics of the fully hadronic channel as 44 percent of all W boson pair decays are semileptonic. The analysis of semileptonic events therefore has a considerable weight in the measurement of the W boson mass.

Chapter 3

Event Simulation

To ensure a proper analysis of real data, physics processes are simulated with so called *Monte Carlo generators*. The analysis is applied to both Monte Carlo and data events. A comparison between both results can be used as a check on the analysis method. Monte Carlo events are generated in two parts. The first part consists of the simulation of primary particles and their subsequent decay, the second part is the simulation of the detector response. The event simulation starts with the generation of primary particles. The particles are produced according to Monte Carlo input parameters and calculated matrix elements. The subsequent *perturbative QCD stage* might result in the emission of gluons. The result is called the *parton level* of the event simulation. Now fragmentation and hadronization are simulated in the *non-perturbative QCD stage*. The resulting particles are passed on to a simulation of the OPAL detector. The paths of the particles through the detector are determined and possible interactions with matter are added along with the simulation of the decay of unstable particles. The detector response to the set of particles thus obtained is now simulated.

3.1 Monte Carlo Generators

Different generators are used in the event simulation at OPAL. Some of the most important are listed in the section below.

KoralW [10]

KoralW is a W boson pair generator. The production of W boson pairs and the corresponding decay processes — including subsequent decays of tau leptons and hadronization — are simulated. The multihadron generator Jetset[1] is included for the simulation of hadronization. Radiative effects like Initial and Final State Radiation and Bremsstrahlung are also taken into account.

[1] described in detail in chapter 3.2

Pythia [11]

Pythia generates QCD processes with two-fermion final states. The program can also be used for the simulation of processes with four-fermion final states. It does not consider interference effects between different diagrams. Pythia is the standard Monte Carlo generator for the simulation of two-fermion background events.

GRC4F [12]

GRC4F is used in the generation of four-fermion processes included in the Standard Model. Two different ways to deal with Initial State Radiation are implemented. The GRC4F code is based on a Feynman diagram automatic computation system, the GRACE system. CKM matrix mixing is not considered in this Monte Carlo generator.

Excalibur [13]

Excalibur is a simulation program for the production of four-fermion processes. The implementation of all four-fermion diagrams — including interference effects between them — is optional. It is also possible to use only selected diagrams. The program itself considers fermions as massless. For the simulation of hadronization, an interface to Jetset provides fermion masses for the generation of initial parton showers.

3.2 Models for Hadronization

Jetset [14]

Jetset was the most widely used multihadron generator at LEP1 and provides a good description of most features of hadronic final states. It uses the Lund model of *string fragmentation*. Within the OPAL collaboration, Jetset is commonly used to perform the hadronization for standard Monte Carlo events.

String Fragmentation

The model of string fragmentation starts with the model of linear confinement: Energy is stored in a colour dipole field between colour charge and colour anticharge of a quark-antiquark pair $q\bar{q}$. The field increases linearly with growing distance between the charges, creating a linearly rising potential. If this potential exceeds a certain value, the string breaks, producing a new quark-antiquark pair $q'\bar{q}'$. We thus obtain two colour-singlet systems: $q\bar{q}'$ and $q'\bar{q}$. These break-up processes will proceed as long as the invariant mass of either string is large enough to produce another quark-antiquark pair.

Herwig [15]

Herwig is another multihadron generator in use at OPAL. In contrast to Jetset, the underlying hadronization model is the model of *cluster fragmentation*. Herwig is mostly used as a postgenerator, taking the 4-vectors of primary leptons and quarks over from other Monte Carlo generators. In this analysis the Herwig generator is used for systematic studies on fragmentation and hadronization.

Cluster Fragmentation

After the perturbative QCD stage, all outgoing gluons are split non-perturbatively into quark-antiquark and diquark-antidiquark pairs. Each jet now consists of a set of outgoing quarks and antiquarks. All final-state colour lines can be followed from a quark-antidiquark to an antiquark-diquark with which it can form a colour-singlet cluster. These clusters are now fragmented into hadrons.

3.3 Detector Simulation

The simulated particles now enter the OPAL detector simulation. This simulation is provided by the GOPAL [16] program, a program using the CERN GEANT package [17]. The GEANT package provides the means to define geometrical parameters of the detector using standard shapes. The tracking of particles inside the detector is simulated along with physical processes like scattering, subsequent decays of particles and interactions with matter. GOPAL thus produces a simulated *detector response* that can be compared to the results we obtain from real data collected at the OPAL detector.

Chapter 4

The OPAL Experiment at LEP

A method to produce the particles described in the Standard Model is the annihilation of matter and antimatter particles in high energy collisions. To achieve this, particles are accelerated and forced to collide, producing particles with properties such as energy, momentum and charge that can be detected quite effectively. On the basis of these studies it is possible to reconstruct decays of Z^0 and W^+/W^- bosons. This method enables physicists working in the field of particle physics to make precise tests of the Standard Model of particles and their interactions.

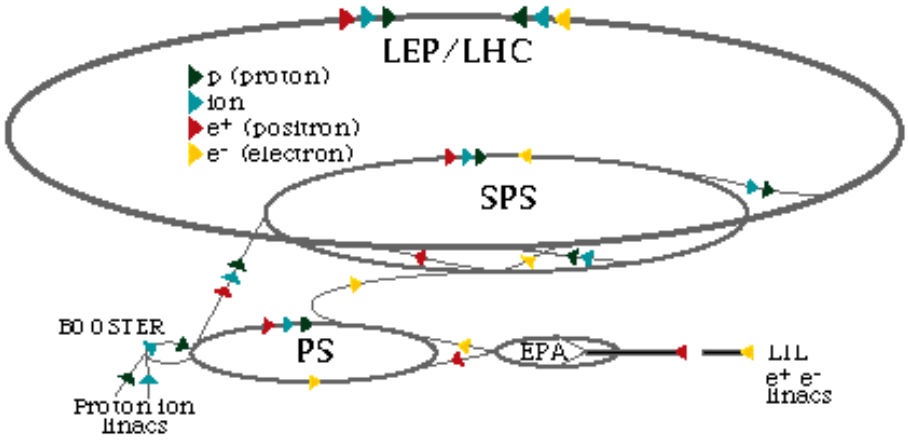

Figure 4.1: *The Accelerator Complex at CERN: PS complex: Proton Synchrotron, accelerates stable charged particles, corresponding antiparticles and heavy ions. SPS: Super Proton Synchrotron: Circular accelerator, originally built to accelerate protons. LEP: Large Electron Positron Collider and (currently under construction) LHC: Large Hadron collider*

The accelerator complex at CERN[1] was constructed to enable these annihilations. It includes particle accelerators and colliders, the **L**arge **E**lectron **P**ositron collider having long been one of the biggest. The whole complex consists of 10 accelerators in total, where beams of electrons and positrons, protons and antiprotons as well as heavy ions such as oxygen, sulphur and lead can be handled. During the process of acceleration, the bunches

[1]European Organization for Nuclear Research

are moving from one machine to another, starting at the smaller linear accelerators and going up to the larger circular colliders including the LEP.

The end of the year 2000 has also brought the end of LEP. In November 2000, the last events were recorded before LEP was closed down to give way to another experiment, the LHC (Large Hadron Collider), that will go up to higher energies and thus allow the search for particles with masses exceeding the masses of W^+/W^- and Z^0 bosons.

4.1 The Large Electron Positron Collider (LEP)

Figure 4.2: *Aerial view of the CERN site just outside Geneva. The large circle indicates the line of the LEP tunnel, 27 km in circumference. The small circle marks the SPS tunnel, 7 km in circumference.*

Located near Geneva in Switzerland, the **L**arge **E**lectron **P**ositron Collider (LEP) at Cern has long maintained its outstanding position as the largest particle accelerator worldwide. In a ring of 27 km in circumference, 100 m beneath the ground, bunches of electrons and positrons were accelerated to a speed bordering the speed of light. The bunches of particles passed the ring in opposite directions. At four symmetric points around the

ring they were focused and thus made to collide. The four LEP experiments ALEPH[2], DELPHI[3], L3[4] and OPAL[5] were located at these points. Even though each bunch contained more than 10^{11} particles, only one in about 40 000 collisions produced a head-on electron-positron-collision. The bunches were therefore made to circulate the ring for hours, passing the collision points more than 10 000 times a second.

4.2 The OPAL Detector

4.2.1 Overview of the Detector

The OPAL experiment started operation in 1989. The end of LEP also meant the end of OPAL, so the last data was taken in November 2000. The detector itself is currently being dismantled, but the analysis of data collected in the last years will still go on for a while.

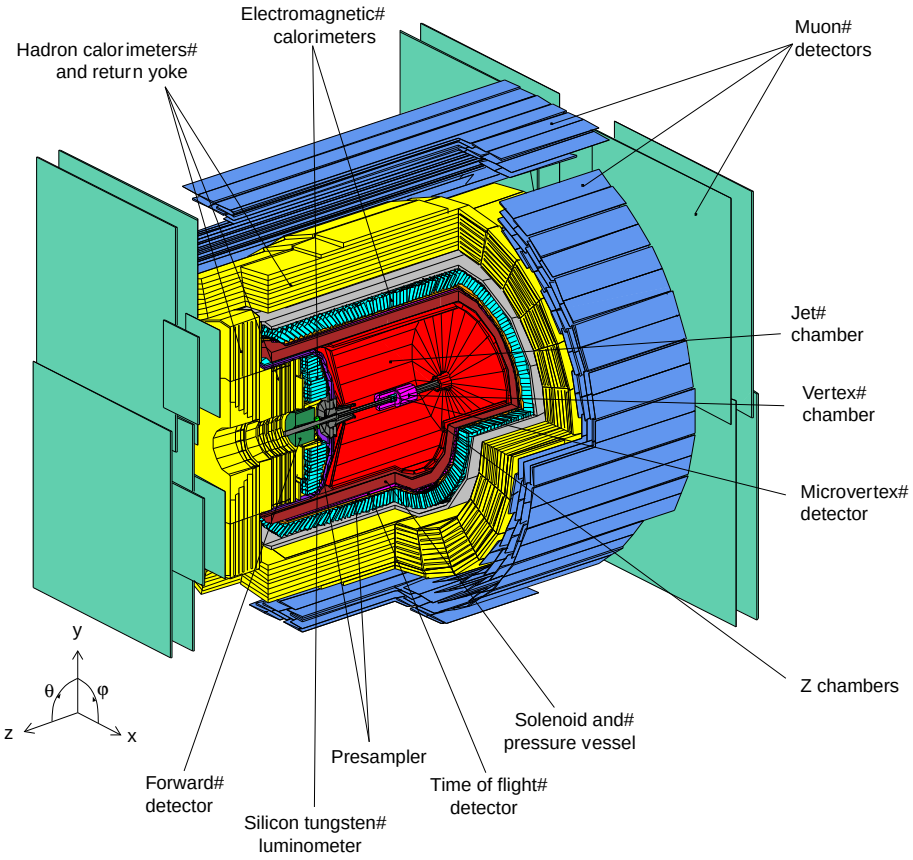

Figure 4.3: *Cut-away view of the OPAL detector*

[2] **A**pparatus for **LE**P **Ph**ysics
[3] **D**etector with **L**epton, **P**hoton and **H**adron **I**dentification
[4] Proposal 3
[5] **O**mni **P**urpose **A**pparatus for **L**EP

As can be seen in figure 4.3, the detector itself consists of a number of elements surrounding the 'heart' of the experiment in different layers. At the centre of the detector, electrons and positrons collide. They come in along the so called beam pipe, an evacuated metal cylinder with a diameter of a few cm passing through the middle of the detector. The results of these electron-positron-collisions are measured in the detector components surrounding the beam pipe. The detector has a length of about 12 m and a diameter of 10 m in total. Starting from the center, the whole detector can roughly be divided into three main parts, the *Tracking System*, the *Calorimeters* and the *Muon Detector*.

The Tracking System

All parts of the Tracking System work in a similar way. Charged particles cause ionisation when passing the low-density material of the detectors. The ionisation electrons can easily be detected in different regions of the Tracking System and thus mark the way the particles are going. The tracking system itself is located within a cylinder symmetric field of 0.435 T oriented along the z-axis (the axial system is depicted in figure 4.3). The field is created by a solenoid encompassing the Jet Chamber.

The whole Tracking System consists of a *Silicon Microvertex Detector*, a *Vertex Detector*, a *Jet Chamber* and *Z-Chambers* (in order of increasing radius). The innermost detector, the *Silicon Microvertex Detector*, is built directly around the beam pipe, close to the interaction point. It consists of silicon wafers processed by conventional integrated circuit manufacturing techniques. When traversing the silicon, charged particles produce both electrons and holes that are sucked into strips running along each wafer. The resulting charge collected on each strip is read out and the exact position of the passing points of the particles can be reconstructed.

The next tracking chamber, the *Vertex Chamber*, is a cylindrical drift chamber of 1 m in length and a diameter of 47 cm. It is segmented radially into an inner layer of 36 cells with axial wires and an outer layer of 36 small angle stereo cells. The axial cells ensure a precise measurement of the position of the tracks in the r-Φ-plane. The position with regard to the z-axis can be determined by measuring the time difference between the signals from the two ends of the anode wire. A combination of both axial and stereo cell information ensures a precise measurement of the z coordinate.

Now we reach the heart of the Tracking System, the *Jet Chamber*. The chamber is 4 m in length with an inner diameter of 0.5 m and an outer diameter of 3.7 m. The sensitive volume is divided into 24 sectors with 159 axial sense wires each and is filled with a gas mixture of argon, methane and isobutane at 4 bar. The ionisation caused by charged particles is measured at different points as they pass the chamber and so their paths can be reconstructed. The Jet Chamber is not only used for the reconstruction of the particle tracks and thus for the precise measurement of the momentum of the particles (see equation (4.2)) but it also allows particle identification on the basis of the specific loss of energy in matter (see equation (4.1)).

The drift chambers are completed by *Z-Chambers* surrounding the Jet Chamber in the form of a barrel layer covering the polar angle from 44 degrees to 136 degrees and almost all of the azimuthal angle. They are designed specifically to enable precise measurements of the z coordinates of the track of charged particles as they leave the Jet Chamber.

Finally, the *Time-of-Flight Detector* (TOF) is located right outside the Tracking System and the magnetic solenoid. It consists of 160 scintillators. Charged particles excite the scintillator material and cause an emission of photons than can be detected by photomultipliers at both ends of the TOF bars. The TOF provides charged particle identification in the range of 0.6 to 2.5 GeV. With its quick response, the Time-of-Flight Detector also represents an important part of the trigger system of the OPAL detector. It is furthermore used as a means to reject cosmic rays.

Calorimeters

The calorimeter system is constructed to measure the energy of both charged and neutral particles produced in electron-positron-collisions. The calorimeters themselve are composed of dense material in which the incoming particles are slowed down and stopped, dispensing their energy to the surrounding medium. So — unlike the Tracking Chambers, whose main design is the measurement of the momentum and direction of charged particles — the calorimeters are built as total absorption detectors. The energy disposed in the calorimeter material can be measured in various ways. As the interaction mechanism of particles with matter strongly depends on whether the particles are subject to the strong force or not, the calorimeter system is subdivided into two main parts, the *Electromagnetic Calorimeter (ECAL)* and the *Hadron Calorimeter (HCAL)*.

Located right between the coil and the return yoke of the magnet, the *Electromagnetic Calorimeter* mostly consists of lead-glass blocks covering 98 percent of the solid angle. It is designed to measure the energies of photons, electrons and positrons. When crossing the high-Z material of the lead-glass blocks, the electrons and photons create an electromagnetic shower caused by a combination of Bremsstrahlung and pair production. Relativistic electrons and positrons within the shower produce Cherenkov photons that are detected via photomultipliers connected to the lead-glass blocks. The number and the pulse height of these photons are directly correlated with the energy of the original particle. An extension of about 22 times the radiation length of the particles insures that the showers always come to an end within the calorimeter. But due to the magnet coil and the pressure vessel, the incoming particles have to traverse about 2 radiation lengths before even reaching the lead-glass blocks. It therefore happens frequently that electromagnetic showers start before entering the calorimeter itself. A Presampler, built of Limited-Streamer tubes and mounted between the Time-of-Flight Detector and the Electromagnetic Calorimeter, compensates for this effect by measuring the amount of showering in the coil. These measurements are then used to improve the energy resolution. The high granularity of the Presampler also improves the discrimination between neutral pions and photons and between electrons and hadrons.

The *Hadron Calorimeter* surrounds the Electromagnetic Calorimeter. It mostly consists of iron, the iron of the magnet return yoke providing 4 or more interaction lengths of absorber material interleaved with layers of streamer chambers. The hadrons lose their energy in inelastic collisions with the heavy nuclei within the passive calorimeter material, the iron. Secondary hadrons emanating from these collisions are then the beginning of hadronic showers. Hadronic showers also contain electromagnetic components such as the decay of neutral pions. As the Electromagnetic Calorimeter already constitutes 2

interaction lengths of material, the hadronic showers can easily start before the particles reach the Hadron Calorimeter. The energy measurement is therefore made in combination with results obtained from the Electromagnetic Calorimeter.

Muon Detectors

The whole OPAL detector is completed by the Muon Detector, a barrel and two endcaps covering the iron yoke almost completely. It consists of four layers of planar drift chambers in the barrel region and limited-streamer tubes in the endcaps. Apart from neutrinos, muons are the only particles that are not absorbed on their way through the calorimeters. Particles detected in the Muon Chambers can thus be classified as muons. The direction of the muons is retrieved by comparing the hit coordinates of different layers. In order to discriminate between primary particles produced in e^+/e^--collisions and secondary muons emanating from calorimeter showers, the hits recorded in the muon system are compared to the information given by the central tracking system. Secondary and cosmic muons are thus excluded.

4.2.2 Particle Identification

Identification of Charged Particles

Particle Identification in the Tracking System

The amount of ionization a given particle produces as it crosses the Jet Chamber depends on the particle type and its momentum. When traversing matter, a charged particle disposes energy along its path the medium amount of which can be described by the Bethe-Bloch formula. The loss of energy is about equally divided into ionization and excitation of the material the particle traverses and is given by

$$\frac{dE}{dx} = \frac{4\pi N e^4 z^2}{mc^2\beta^2}\left(\ln\frac{2m_e c^2\beta^2\gamma^2}{I} - \beta\right) \tag{4.1}$$

where e denotes the elementary charge, m_e the mass of the electron, c the speed of light, N the density of electrons in the given matter, z the charge of the ionizing particle, $\beta = \frac{v}{c}$ the scaled velocity of the particles, $\gamma = \sqrt{\frac{1}{1-\beta^2}}$ the Lorentz factor and I the effective ionisation potential. I basically depends on the atomic number Z: $I \approx 16 \cdot Z^{0.9}\ eV$. The measurement of the energy loss in matter can thus be used to identify particles in some energy regions.

Electron Identification

Highly energetic electrons are identified in the Electromagnetic Calorimeter. Clusters in the ECAL with a significant amount of energy along with a corresponding track in the Tracking System indicate the occurrence of an electron.

Muon Identification

Muons are — apart from the undetectable neutrinos — the only particles produced in e^+/e^--collisions that are not absorbed within the high-density material of the different calorimeters. The method to identify a muon in the Muon Detector is therefore quite obvious: All particles detected within the Muon Chambers with corresponding tracks recorded in the Central Tracking System are considered as muons.

Identification of Neutral Particles

Photons are identified by using both information from the Tracking System and from the Electromagnetic Calorimeter. Being neutral particles, photons cannot be detected in drift chambers. They do not leave tracks within the Tracking System of the OPAL detector. But they do interact with the high-density material of the Electromagnetic Calorimeter. Hits in the ECAL without corresponding tracks in the Tracking System can thus be identified as photons. Neutral pions decay further into photons ($\pi^0 \rightarrow 2\gamma$) that are detected as described above. Two detected photons with an invariant mass equal to the mass of the π^0 indicate the occurrence of this particle.

4.2.3 Measurement of Energy and Momentum

Charged Particles

When passing the low-density material of one of the drift chambers included in the *Tracking System*, a charged particle causes ionization along its path. The chambers are inclosed in a cylindric magnetic field forcing charged particles on a circular track. The curvature can be measured and from this information we deduce the *momentum* of the charged particle as the radius of its track within a magnetic field is given by

$$R = \frac{pc}{qB} \tag{4.2}$$

where p denotes the momentum of the charged particle, c the speed of light, q the charge of the particle and finally B the strength of the magnetic field.

The energy of a charged particle is given by the amount of energy it disposes within the Electromagnetic Calorimeter. As previously described in the section above, charged particles produce electromagnetic showers. Relativistic electrons and positrons originating from these showers now produce Cherenkov photons detected via photomultipliers. A direct correlation between number and pulse height of these photons on one hand and the energy of a given particle on the other hand allows the reconstruction of this energy.

Neutral Particles

As already described in the section above, *photons* are stopped within the Electromagnetic Calorimeter, disposing their energy to the surrounding medium. The original energy of the photons can thus be retrieved. The neutral pions decay into photons, their energy is determined as described above.

Chapter 5

Selection and Reconstruction of Semileptonic Events

The first step in each analysis is the search for a possible candidate, in this special case the search for a semileptonic W boson pair decay candidate. When detected, a certain event leaves a characteristic signature in the detector. Only events matching the special signature expected from semileptonic W boson pair decays are further analysed. The event selection used in this analysis is described in detail in the following chapter 5.1. The next step is the reconstruction of the previously selected events. The most probable lepton candidate is determined and the non-leptonic part of tracks and calorimeter clusters are combined to form two jets. The reconstruction of tau leptons needs special care. Due to the subsequent decay of the tau lepton it is impossible to measure energy and momentum of the tau lepton directly. The event reconstruction is described in chapter 5.2. Now a kinematic fit is applied to the reconstructed jet and lepton momenta. The kinematic fit takes constraints like the conservation of energy and momentum into account and yields an improved estimation of the momenta of primary decay products. This information can be used in the calculation of the invariant mass of the W boson for each single event.

5.1 Selection of Semileptonic Events

The semileptonic decay of a W boson pair ($W^+W^- \rightarrow \mathrm{q\bar{q}}l\bar{\nu}$) is characterized by two hadronic jets and an isolated track marking the path of the lepton. An associated calorimeter cluster in the ECAL indicates an electron. A low multiplicity jet can be observed in the case of a tau lepton due to its further decay into hadrons. And a hit in the muon detector identifies the lepton as a muon. In all semileptonic decay channels one expects missing energy carried away by the undetected neutrino. An event is selected as semileptonic if its signature in the detector meets these expectations. A typical semileptonic event display is shown in figure 5.1.

The event selection is carried out in different stages. We start with matching the event against the hypothesis of a fully leptonic event as this is the event class with the clearest signature in the detector: two acoplanar, energetic leptons and a large amount of missing energy and momentum due to the undetected neutrinos. Low multiplicity jets can be

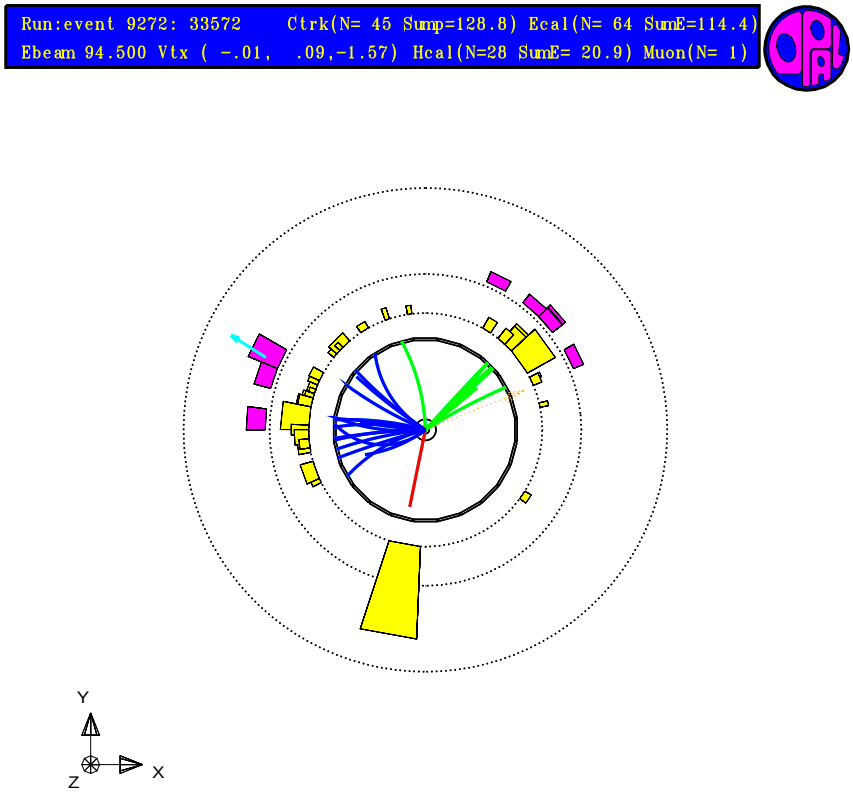

Figure 5.1: *OPAL event display showing a semileptonic event. Blue and green lines denote the jet tracks detected in the Central Tracking Detector, yellow blocks are hits in the ECAL and pink blocks mark entries in the HCAL. The dashed arrow indicates the direction of the missing momentum of the undetected neutrino.*

observed if one (or both) of the leptons happens to be a tau lepton. Events that do not match the fully leptonic hypothesis are tested against the hypothesis of a semileptonic event: two hadronic jets and an isolated track marking the path of the lepton respectively a low multiplicity jet in the case of a hadronically decaying tau lepton. Only events failing both the fully leptonic and the semileptonic selection are tested against the hypothesis of a fully hadronic event, the event class with the least clear signature: Four or more jets are observed. The center-of-mass energy of a fully hadronic event is converted completely into hadrons. This analysis deals with the *selection of semileptonic events* [19].

The selection of semileptonic events can roughly be divided into three main parts:

- The **Likelihood Selection** including relative likelihood cuts. These cuts largely reduce the dominant two-fermion background while maintaining a high efficiency for signal events.
- The **rejection of four-fermion background** including cuts to reduce background from different four fermion processes:
  $e^+e^- \to Z^0Z^0, e^+e^- \to We\nu_e$ and $e^+e^- \to Z^0e^+e^-$
- The **Trackless Selection** finally recovers events which fail the likelihood selection due to the absence of a track that can be associated with the lepton.

5.1.1 The Likelihood Selection

When dealing with the leptonic part of semileptonic W boson pair decays, six different decay chains have to be considered: The decays into electron, muons

$$W \to e\nu_e \quad , \quad W \to \mu\nu_\mu$$

and tau leptons further decaying into a lepton-neutrino pair,

$$W \to \tau\nu_\tau \to e\nu_e\nu_\tau \quad , \quad W \to \tau\nu_\tau \to \mu\nu_\mu\nu_\tau \ ,$$

or into hadrons, one charged hadron h, usually $\pi^\pm$ or $K^\pm$, n neutral π^0 mesons and a neutrino respectively three charged hadrons h, n neutral π^0 mesons and a neutrino,

$$W \to \tau\nu_\tau \to h(n\pi^0)\nu_\tau\nu_\tau \quad , \quad W \to \tau\nu_\tau \to 3h(n\pi^0)\nu_\tau\nu_\tau \ .$$

The likelihood selection consists of six selections running in parallel. Each one is optimized following one of the decay chains mentioned above.

Before the Likelihood Selection itself is applied, the events are subjected to *track and cluster quality cuts* [19] to remove fake signals from electric noise in the Tracking System and the calorimeters. Furthermore, obvious background events like two-photon events and low multiplicity events contradicting the assumption of two primary quarks are excluded by demanding a minimum number of charged tracks and clusters in the ECAL and a minimum visible energy. Events passing these rather loose selections are considered as possible $W^+W^- \to \mathrm{q\bar{q}}l\bar{\nu}$ candidates. They are now subjected to the Likelihood Selection itself. It starts with the determination of the most probable lepton candidate:

Identification of the Lepton Candidate

The track most consistent with originating from a leptonic W boson decay is selected. The identification of the best lepton track is carried out as follows: For each of the six decay chains a probability is calculated considering energy and momentum as well as the spatial isolation of the track. The track with the highest probability is taken as the lepton track.

The Preselection

Just like the lepton identification, the preselection is carried out separately for each of the six possible decay chains. It already removes a large part of the background (especially events clearly originating from $Z^0 \to \mathrm{q\bar{q}}$) before the events enter the Likelihood Selection. The preselection is carried out as follows: The best lepton candidate is used as a basis to determine the kinematic properties of the event. The track corresponding to the lepton candidate is removed, the remaining tracks and calorimeter clusters are forced into two jets. As charged particles are detected in both the Tracking System and the calorimeters, the jet energies have to be corrected for double counting. In the end, the lepton and its corresponding energy are added back to the event. Now several cuts are applied, taking variables like the visible energy, the energy and momentum of the lepton candidate, the track multiplicity, the highest energy of an isolated photon, the invariant mass, the probability of the lepton identification and the angle between the momentum of the lepton and the direction of missing momentum into account. Only events failing both the $W^+W^- \to \mathrm{q\bar{q}}e\bar{\nu}_e$ and the $W^+W^- \to \mathrm{q\bar{q}}\mu\bar{\nu}_\mu$ preselection are subjected to the $W^+W^- \to \mathrm{q\bar{q}}\tau\bar{\nu}_\tau$ preselection.

Relative Likelihood Selections

After the preselection, the $Z^0/\gamma \to \mathrm{q\bar{q}}$ background is already reduced by a factor of about ten. Now a *relative likelihood method* is applied to reduce the dominant $e^+e^- \to \gamma \to \mathrm{q\bar{q}}$ background by another factor of 100. The relative likelihood method consists of six likelihood selections — again one for each decay chain. The relative likelihood selection — as well as the preselection described in the section above — only passes events failing the $W^+W^- \to \mathrm{q\bar{q}}e\bar{\nu}_e$ and $W^+W^- \to \mathrm{q\bar{q}}\mu\bar{\nu}_\mu$ selection on to the $W^+W^- \to \mathrm{q\bar{q}}\tau\bar{\nu}_\tau$ selection. $W^+W^- \to \mathrm{q\bar{q}}\tau\bar{\nu}_\tau$ events that are wrongly selected by one of the other selections are recovered at a later stage. The $W^+W^- \to \mathrm{q\bar{q}}l\bar{\nu}_l$ likelihood is based on a set of variables x_i comparing observed values to expected Monte Carlo distributions. This set of variables includes variables related to the energy or momentum of the lepton candidate and its isolation, the lepton identification probability and global properties like the visible energy as well as variables related to the topology of the event like the angles between the lepton and the nearest jet or the vector of the missing momentum. This method yields a corresponding set of probabilities $P(x_i)$ for each individual variable. The likelihood $L_{q\bar{q}l\bar{\nu}_l}$ is given by the product of these probabilities. Monte Carlo distributions for $Z^0/\gamma \to \mathrm{q\bar{q}}$ events are used to determine the background likelihood. The relative likelihood $\mathcal{L}_{q\bar{q}l\bar{\nu}_l}$ can be written as

$$\mathcal{L}_{q\bar{q}l\bar{\nu}_l} = \frac{L_{q\bar{q}l\bar{\nu}_l}}{L_{q\bar{q}l\bar{\nu}_l} + \mathrm{f} \times L_{q\bar{q}}} \tag{5.1}$$

where f denotes the ratio of the preselected $\mathrm{q\bar{q}}$ background cross-section to the signal cross-section, both obtained from Monte Carlo studies. Events with a likelihood exceeding 0.5 are selected.

Rejection of Four Fermion Background

After the likelihood selections, the main four-fermion background sources are:

- $q\bar{q}\mu^+\mu^-$ and $q\bar{q}\tau^+\tau^-$ events that are wrongly selected as $W^+W^- \to q\bar{q}\mu\bar{\nu}_\mu$ or $W^+W^- \to q\bar{q}\tau\bar{\nu}_\tau$ events
- $q\bar{q}e^+e^-$ events originating from Z^0Z^0 decays that are selected as $W^+W^- \to q\bar{q}e\bar{\nu}_e$
- single W background and $q\bar{q}\nu\bar{\nu}$ events selected as $W^+W^- \to q\bar{q}\tau\bar{\nu}_\tau$ events

These background events are removed with cuts taking the specific signature of each background process into account. This procedure is described in detail in [19]. Table 5.1.1 shows the reduction of the cross-sections of four-fermion background effects achieved by the application of these cuts.

background process	cross section before 4f rejection cuts (fb)	cross section after 4f rejection cuts (fb)
$e^+e^- \to q\bar{q}e^+e^-$	141	78
$e^+e^- \to q\bar{q}\mu^+\mu^-$	80	27
$e^+e^- \to q\bar{q}\tau^+\tau^-$	44	41
$e^+e^- \to We\bar{\nu}_e$	178	70

Table 5.1: *Cross-sections of four-fermion background processes passing the* $W^+W^- \to q\bar{q}l\bar{\nu}_l$ *likelihood cuts before and after the application of four-fermion rejection cuts [19].*

Event Categorisation

A non-negligible part of events in each channel are selected wrongly or by more than one of the six likelihood selection. Table 5.2 shows the fraction of semileptonic events selected in the different likelihood selections. About four percent of the $W^+W^- \to q\bar{q}e\bar{\nu}_e$ and $W^+W^- \to q\bar{q}\mu\bar{\nu}_\mu$ events pass both selections and about 33 percent of the $W^+W^- \to q\bar{q}\tau\bar{\nu}_\tau$ pass one of these selections as well.

	likelihood selection			
decay channel	$q\bar{q}e\bar{\nu}_e$	$q\bar{q}\mu\bar{\nu}_\mu$	$q\bar{q}e\bar{\nu}_e$ and $q\bar{q}\mu\bar{\nu}_\mu$	$q\bar{q}\tau\bar{\nu}_\tau$
$e^+e^- \to W^+W^- \to q\bar{q}e\bar{\nu}_e$	0.860	0.042	0.038	0.029
$e^+e^- \to W^+W^- \to q\bar{q}\mu\bar{\nu}_\mu$	0.044	0.876	0.038	0.029
$e^+e^- \to W^+W^- \to q\bar{q}\tau\bar{\nu}_\tau$	0.188	0.160	0.012	0.466

Table 5.2: *Situation after the application of the six likelihood selections: Fractions of semileptonic events* $W^+W^- \to q\bar{q}l\bar{\nu}_l$ *passing the likelihood selection* $q\bar{q}l\bar{\nu}_l$ *[19].*

To avoid ambiguities, the events are subjected to an additional set of relative likelihoods in the categorisation stage of the semileptonic event selection. Again, likelihood discriminants are used in the four different levels of categorisation. $W^+W^- \to q\bar{q}\tau\bar{\nu}_\tau$ events selected wrongly as $W^+W^- \to q\bar{q}e\bar{\nu}_e$ or $W^+W^- \to q\bar{q}\mu\bar{\nu}_\mu$ events are recovered at this stage. The four levels are applied successively in the following order:

- Events passing both the $q\bar{q}e\bar{\nu}_e$ and the $q\bar{q}\mu\bar{\nu}_\mu$ likelihood cuts are categorized either as $W^+W^- \to q\bar{q}e\bar{\nu}_e$ or $W^+W^- \to q\bar{q}\mu\bar{\nu}_\mu$
- Events passing the $q\bar{q}e\bar{\nu}_e$ likelihood cut are classified as one of the following: $W^+W^- \to q\bar{q}e\bar{\nu}_e$, $W \to \tau\nu_\tau \to e\nu_e\nu_\tau$ or $W \to \tau\nu_\tau \to h(n\pi^0)\nu_\tau\nu_\tau$
- Events passing the $q\bar{q}\mu\bar{\nu}_\mu$ event selection are classified as $W^+W^- \to q\bar{q}\mu\bar{\nu}_\mu$, as $W \to \tau\nu_\tau \to \mu\nu_\mu\nu_\tau$ or as $W \to \tau\nu_\tau \to hn\pi^0\nu_\tau$ events.
- Events passing more than one of the four $q\bar{q}\tau\bar{\nu}_\tau$ likelihood cuts are classified as one of the four $W^+W^- \to q\bar{q}\tau\bar{\nu}_\tau$ decay chains.

Table 5.3 shows the situation after the categorisation stage. The percentage of wrongly selected semileptonic events — especially in the $q\bar{q}\tau\bar{\nu}_\tau$ channel — has been largely reduced.

	likelihood selection		
decay channel	$q\bar{q}e\bar{\nu}_e$	$q\bar{q}\mu\bar{\nu}_\mu$	$q\bar{q}\tau\bar{\nu}_\tau$
$e^+e^- \to W^+W^- \to q\bar{q}e\bar{\nu}_e$	0.841	0.020	0.051
$e^+e^- \to W^+W^- \to q\bar{q}\mu\bar{\nu}_\mu$	0.010	0.855	0.055
$e^+e^- \to W^+W^- \to q\bar{q}\tau\bar{\nu}_\tau$	0.041	0.039	0.722

Table 5.3: *Situation after the application of both the six likelihood selections and the likelihood discriminants of the categorisation stage [19].*

5.1.2 The Trackless Selection

The trackless selection is designed to recover events without a corresponding lepton track in the Central Tracking System. The lepton might either be beyond the tracking acceptance of the OPAL detector or within but no associated track was reconstructed. Two trackless selections, one for $q\bar{q}e\bar{\nu}_e$ and one for $q\bar{q}\mu\bar{\nu}_\mu$ events, are applied to include these events as well. Both selections search for isolated ECAL clusters indicating an isolated lepton which is not associated with a WW-quality track. Further information is then used to tag the isolated calorimeter cluster as a possible lepton candidate, a lepton *blob*. In addition to the requirements mentioned above, a significant amount of energy must be deposited in the ECAL to identify the cluster as an electron blob. The identification of a muon blob requires evidence of a minimum ionizing particle (MIP) in the muon chambers or the hadron pole-tip calorimeter.

5.2 Reconstruction of Semileptonic Events

Events passing the semileptonic event selection are now considered as $W^+W^- \to q\bar{q}l\bar{\nu}_l$ candidates and reconstructed accordingly. The semileptonic W boson pair decay consists of a leptonic part, where the W boson decays into a lepton-neutrino pair leaving one charged track or a low multiplicity jet originating from the subsequent hadronic decay of a primary tau lepton, and a hadronic part, where the W boson decays into a quark-antiquark pair finally leading to two high multiplicity jets. The reconstruction of both

parts is given below along with a description of the special treatment one has to apply on the reconstruction of tau and trackless events.

5.2.1 The Leptonic Part

The leptonic part of a semileptonic W boson pair decay follows one of the decay chains already mentioned in chapter 5.1.1:

$$
\begin{array}{ll}
W \to e\nu_e & \text{(I)} \\
W \to \mu\nu_\mu & \text{(II)} \\
W \to \tau\nu_\tau \to e\nu_e\nu_\tau & \text{(III)} \\
W \to \tau\nu_\tau \to \mu\nu_\mu\nu_\tau & \text{(IV)} \\
W \to \tau\nu_\tau \to h(n\pi^0)\nu_\tau\nu_\tau & \text{(V)} \\
W \to \tau\nu_\tau \to 3h(n\pi^0)\nu_\tau\nu_\tau & \text{(VI)}
\end{array}
$$

The identification of the most probable lepton candidate is already completed in the semileptonic event selection. The leptonic part now consists of a single track in the Central Tracking System and an associated calorimeter cluster (decay chains I to IV) or of one (V) or three (VI) charged hadronic tracks and the corresponding clusters in the calorimeter. The kinematic properties — energy, momentum and direction — are determined as follows: The energy of an *electron* (originating from I or III) is measured in the Electromagnetic Calorimeter as the resolution of the ECAL exceeds the resolution of the Central Tracking System when it comes to highly energetic electrons. The direction of the electron is given by its track in the Tracking System. Muons (originating from II or IV) generally pass the detector without much interaction with the calorimeter material. Information on both momentum and direction are therefore taken from the Central Tracking System. Tau leptons produced in W boson pair decays are highly energetic. One can therefore assume that the decay products of the tau lepton maintain its original direction. In the case of hadronic decays of tau leptons, the energy of the primary tau lepton is estimated by the sum of the momenta of the tracks associated with the best tau candidate and any unassociated calorimeter clusters within a certain region encircling the original tau direction. This direction is given by the tracks measured in the Central Tracking System. The energy of tau events thus obtained cannot be used to reconstruct the energy of the primary tau lepton as an unknown part is carried away by neutrinos. But it is needed to ensure a proper event selection.

5.2.2 The Non-Leptonic Part

To distinguish between the leptonic and the non-leptonic part of an event, all tracks and clusters associated with the best lepton candidate are removed, leaving the non-leptonic part. The remaining tracks and clusters are forced into two jets using the Durham algorithm [20], a standard jet finder for W boson pair analyses within the OPAL collaboration. It combines two tracks (i and j) using jet separation parameters defined as

$$
y_{ij} = \frac{2\,min\,(E_i^2, E_j^2)}{s}(1 - cos(\theta_{ij}))\ , \tag{5.2}
$$

where E_i and E_j denote the energies of the corresponding tracks, $\sqrt{s}$ the center-of-mass energy and θ_{ij} the angle between the two tracks. y_{ij} is calculated for each track and the two tracks with the smallest value of y_{ij} — tracks close to each other or a pair of tracks where at least one track has low energy — are combined to form a new track until only two jets remain.

The measurement of energy and momentum of the jets is rather difficult. In hadronic final states about 2/3 of all energy is carried by charged particles. Tracking generally achieves a higher resolution in both energy and angle measurement than calorimetry. The measurement of the energy of a highly energetic electron is an exception to this rule, but electrons rarely belong to jets. The energy of neutral particles must be determined in the calorimeters as they leave no tracks in the Central Tracking System. But to measure the energy of neutral particles in the calorimeter correctly, the energy deposits of charged particles have to be removed. That is the difficult part of the energy measurement since both charged and neutral particles are intermixed in a narrow space region and cannot be separated by the calorimeters. To solve this problem this analysis uses a *matching* algorithm, the MT package [21]. The algorithm starts with the association (the matching) of tracks and clusters using several criteria such as the position of tracks extrapolated to the calorimeters, the position of cluster center and cluster boundary and cluster energy and expected energy response of the calorimeters for charged particles (calculated from the track momentum). After the matching, clusters with energies within a certain tolerance around the value calculated from their associated tracks are removed. Only their tracks are accepted for the energy measurement. Clusters with energies exceeding the expected energy are reduced by this amount. Unassociated tracks and clusters are fully accepted. The 4-momenta of the jets are now calculated as the sum of the 4-momenta of all tracks included in each jet by the jet finder algorithm described above. It is generally possible to calculate the invariant mass of the W boson (equation 5.10) from the jet momenta thus obtained. The method will be explained later on. But a constraint kinematic fit that uses both the momenta of the jets and the lepton and the corresponding measurement errors as input parameters achieves a much better resolution and is therefore used in this analysis (see chapter 5.3.1 for details).

5.2.3 Tau Events

The reconstruction of $W^+W^- \to \mathrm{q\bar{q}}\tau\bar{\nu}_\tau$ events calls for special care as the primary tau lepton cannot be measured directly but only via the observation of its decay products. The undetected escape of neutrinos carrying an unknown amount of energy further complicates matters. In addition to that, hadrons originating from $W \to \tau\nu_\tau \to h(n\pi^0)\nu_\tau\nu_\tau$ and $W \to \tau\nu_\tau \to 3h(n\pi^0)\nu_\tau\nu_\tau$ decays can mix with hadrons belonging to the non-leptonic part of the W boson pair decay. As a consequence of these effects, the lepton candidate is often misidentified. In about 22 percent of events in which the tau decays hadronically the event selection algorithm errs in the identification of the lepton candidate. This effect leads to an additional background that has to be considered in the reconstruction of tau events, the so called *evil tau* background. *Evil tau events* are events for which the reconstructed tau direction deviates more than 15 degrees from the true tau direction. These events contain no mass information and cannot be used for measurements of the mass of the W boson. As they pass the selection nevertheless, they distort the mass distribution of the

W bosons and have to be treated as an additional background source. To recuperate at least some of the evil tau events another specialized likelihood selection is applied after the event selection, using variables like the momentum of the tau track, the energy deposited in the ECAL, the minimum angle between the two jets of the non-leptonic part of the W boson pair decay and the minimum angle between the tau direction and the nearest jet (see [22] for details). Furthermore, events passing the event selection with a likelihood of 0.4 and less are reclustered into three jets (again using the Durham algorithm). The jet with the lowest energy is now taken as the best lepton candidate if it consists of no more that six charged tracks. Monte Carlo studies show that this *evil tau rejection* results in a shift of events from the high mass region of the mass distribution to the peak region and thus improves the resolution of the mass measurement in the $q\bar{q}\tau\bar{\nu}_\tau$ channel.

5.2.4 Trackless Events

Events without a corresponding lepton track in the Central Tracking System passing the event selection as trackless $W^+W^- \to q\bar{q}e\bar{\nu}_e$ and $W^+W^- \to q\bar{q}\mu\bar{\nu}_\mu$ are nevertheless used in the measurement of the W boson mass.

- **Trackless electrons** still contain energy information. The only difference to electrons with an associated track is the fact that now both the energy and the direction of the electron are taken from entries in the Electromagnetic Calorimeter. They are therefore included in the $W^+W^- \to q\bar{q}e\bar{\nu}_e$ class.
- **Trackless muons** contain practically no energy information. Their direction is determined using information from the Electromagnetic and the Hadron Calorimeter. They are assigned to the $W^+W^- \to q\bar{q}\tau\bar{\nu}_\tau$ class.

5.3 The Invariant Mass of the W Boson

In this analysis a *constrained kinematic fit* is used to determine the invariant mass of the W boson. This method allows the calculation of best estimates to a set of variables while satisfying the equations of constraint such as the conservation of energy and momentum. The following section explains the general method, while the different methods of the implementation of equations of constraint are demonstrated later on.

5.3.1 The Kinematic Fit in Principle

The kinematic fit uses the jet and lepton momenta, the jet and lepton directions and their errors as input values to the calculation of the best estimate of the measured quantities. To achieve this, the deviations of parameters from their corresponding measured values, weighted with the measurement errors, are minimized simultaneously. This analyis uses a least square fit or χ^2 fit for this purpose. The χ^2 function is given by

$$\chi^2 = \sum_{ij} (\vec{p}_{meas} - \vec{p})_i \, V_{ij}^{-1} \, (\vec{p}_{meas} - \vec{p})_j + constraints \tag{5.3}$$

where $\vec{p}_{meas}$ contains the measured momentum of both jets and the lepton and $\vec{p}$ the estimates for these variables. V^{-1} is the inverse covariance matrix implementing the errors of the measured parameters. The diagonal elements of this matrix are the squared standard deviations of the corresponding kinematic variables, the off-diagonal elements are given by the product of the corresponding standard deviations and a correlation factor between the vector components. Possible correlations between the parameters are thus taken into account. Additional factors are added to ensure that the equations of constraint are fulfilled. The minimization of the χ^2 function with regard to these parameters now yields the best estimates while ensuring that the equations of constraint are satisfied. In the semileptonic channel the estimates for the jet and lepton momenta in combination with the conservation of energy and momentum provide us with enough information to calculate the invariant mass of the W bosons. The equations of constraint yield the momentum of the undetected neutrino. Nevertheless, another equation of constraint is applied, the *equal mass constraint*: It is assumed that the masses of both W bosons are equal.

$$m_{W^+} = m_{W^-} \tag{5.4}$$

Studies have shown that the resolution of the event mass is further optimized by the application of the equal mass constraint. The statistical errors are reduced while the systematic errors remain the same (see [23] for details).

The best estimates for the measured values are used along with the equations of constraint to calculate the invariant masses of the two primary W bosons that are forced eqaul. The conservation of momentum thereby yields the momentum of the undetected neutrino.

5.3.2 Implementation of Constraints

There are different ways to include the equations of constraint, the equal mass constraint (equation (5.4)) and the conservation of energy and momentum that is given by

$$\sum_{i=1}^{4}(E_i, \vec{p}_i) = (\sqrt{s}, \vec{0}) \ , \tag{5.5}$$

in the χ^2 function (equation (5.3)). E_i denotes the energy of the i-th particle or jet, $\vec{p}_i$ its momentum and $\sqrt{s}$ the center-of-mass energy. Two methods, one implementing penalty functions and another using Lagrange multipliers to ensure the fulfillment of the equations of constraint, are described in the following.

Penalty Function

Constraints can be included in the χ^2 function in the form of so called *penalty functions*. To obtain these functions the equations of constraint are rewritten to match the following form:

$$f_i(\vec{p}) = 0 \tag{5.6}$$

Their squares, divided by the squared *penalty factors* δ_E and δ_m, are now added to the first part of the χ^2 function (equation (5.3)), yielding the complete χ^2 function:

$$\chi^2 = \sum_{ij} (\vec{p}_{meas} - \vec{p})_i \, V_{ij}^{-1} \, (\vec{p}_{meas} - \vec{p})_j + \frac{(\sum_i E_i - \sqrt{s})^2}{\delta_E^2} + \frac{(m_{12} - m_{34})^2}{\delta_m^2} \tag{5.7}$$

Again $\vec{p}_{meas}$ and $\vec{p}$ are vectors containing the measured and the estimated momenta of the jets and the lepton. V^{-1} denotes the inverse covariance matrix, E_i the energy of the i-th jet or lepton and $\sqrt{s}$ the center-of-mass energy. m_{12} and m_{34} are the masses of the two W bosons W^+ and W^-. Their values are calculated in the following. The minimization of equation (5.7) yields the best approximations of the kinematic variables to the measured values and guarantees that the equations of constraint (5.4) and (5.5) are satisfied. The energy of the i-th jet or lepton is given by

$$E_i = \sqrt{m^2 + \vec{p}^{\,2}} \tag{5.8}$$

where m denotes the measured jet or lepton mass and $\vec{p}$ the corresponding momentum. The mass of the neutrino is assumed to be zero. The conservation of momentum is used in the calculation of the unmeasured neutrino momentum:

$$\vec{p}_\nu = -\vec{p}_{lepton} - \sum_{i=1}^{2} \vec{p}_{jet_i} \tag{5.9}$$

And finally the kinematic variables thus obtained yield the invariant masses of the two W bosons:

$$m_{ij} = \sqrt{(E_i + E_j)^2 - (\vec{p}_i + \vec{p}_j)^2} \tag{5.10}$$

E_i, E_j and $\vec{p}_i, \vec{p}_j$ are the energies and momenta of the two jets in the non-leptonic part and the energies and momenta of the lepton and the neutrino in the leptonic part of the W boson pair. The mass of the neutrino is assumed to be zero.

This analysis implements penalty functions in the kinematic fit and uses MINUIT [24], a CERN package designed to find the minimum value of a multi-parameter function, for the minimization of the χ^2 function. This method proves to work reliably, but the interpretation of the systematic error associated with the penalty functions needs special care. The implementation of penalty functions leads to a systematic error that depends on the choice of the penalty factors. But the impact of this additional systematic error on the total systematic measurement error is comparatively low and can be neglected (see [1], appendix B, for details).

Lagrange Multipliers

The most fundamental method to include equations of constraint in the χ^2 function is the introduction of *Lagrange multipliers* [25]. Like before, the equations of constraint are written in the form of equation (5.6). For each equation of constraint, a new parameter λ_i, the Lagrange multiplier, is introduced. The χ^2 function is now given by

$$\chi^2 = \sum_{ij} (\vec{p}_{meas} - \vec{p})_i \, V_{ij}^{-1} \, (\vec{p}_{meas} - \vec{p})_j + 2\,(\lambda_1(\sum_i E_i - \sqrt{s})^2 + \lambda_2(m_{12} - m_{34})) \quad (5.11)$$

or, written in a shorter form, by

$$\chi^2 = \sum_{ij} (\vec{p}_{meas} - \vec{p})_i \, V_{ij}^{-1} \, (\vec{p}_{meas} - \vec{p})_j + 2 \sum_i \lambda_i f_i(\vec{p}) \quad (5.12)$$

where $f_i(\vec{p})$ denotes the i-th equation of constraint. The derivation of (5.11) with regard to both the kinematic variables p_i and the Lagrange multipliers λ_i yields the following set of equations

$$\frac{\delta\chi^2}{\delta\vec{p}_i} = 2 \sum_i V_{ij}^{-1} \, (\vec{p}_j - \vec{p}_i) + 2 \sum_i \lambda_i \frac{\delta f_i(\vec{p})}{\delta\vec{p}_i} = 0 \quad (5.13)$$

and

$$\frac{\delta\chi^2}{\delta\lambda_i} = f_i(\vec{p}) = 0 \quad (5.14)$$

from which both the Lagrange multipliers and the best estimates for the jet and lepton momenta can be obtained. The consistence between equation (5.14) and (5.6) shows that the equations of constraint are satisfied in this method. The application of equation (5.10) yields the invariant mass of the two W bosons.

During this analysis attempts have been made to replace the penalty functions in the kinematic fit with this fundamental method to avoid a systematic error inherent in the implementation of penalty functions. Unfortunately, the use of Lagrange multipliers in combination with MINUIT does not yield stable results. So another approach was made using a completely different program designed to carry out constraint fits, the Blobel fit routine [26]. The use of Lagrange multipliers is already implemented in the Blobel fit. But this method proves to be inferior to the use of MINUIT in combination with penalty functions in the kinematic fit as well. A detailed description on the subject will be presented in chapter 7.1.

5.3.3 The Fit Probability

The minimum value of the χ^2 function can be used as a measure to the *goodness-of-fit*. As a criterion, the *fit probability* $P_{\chi^2}(\mathcal{N})$ is calculated using the value of the χ^2 function and the number of degrees of freedom of the kinematic fit. To obtain the number of

degrees of freedom one has to take the number of measured parameters, add the number of constraints and reduce it by the number of unmeasured parameters. The number of degrees of freedom $\mathcal{N}$ can be written as

$$\mathcal{N} = \mathcal{N}_{meas} - \mathcal{N}_{unmeas} + \mathcal{N}_{constraints} \tag{5.15}$$

In the semileptonic channel we thus get two degrees of freedom in the $q\bar{q}e\bar{\nu}_e$ and in the $q\bar{q}\mu\bar{\nu}_\mu$ channel: 9 measured parameters: the jet and lepton momenta. 12 fit parameters: the jet and lepton momenta and the momentum of the unobserved neutrino. And finally 5 equations of constraint, the conservation of energy and momentum and the equal mass constraint. This fit is accordingly called 2C fit. In the $q\bar{q}\tau\bar{\nu}_\tau$ channel — due to the subsequent decay of the tau lepton — the direction, but not the energy of the primary tau lepton is measured. So there are only 8 measured parameters but the same number of fit parameters and constraints as in the other semileptonic decay channels. This effect reduces the number of degrees of freedom to 1. The fit in the $q\bar{q}\tau\bar{\nu}_\tau$ channel is therefore called 1C fit.

The fit probability $P_{\chi^2}(\mathcal{N})$ is given by

$$P_{\chi^2}(\mathcal{N}) = \int_{\chi^2}^{\infty} \frac{x^{(\mathcal{N}-2)}\ e^{\frac{x}{2}}}{\sqrt{2^{\mathcal{N}}}\ \Gamma(\frac{\mathcal{N}}{2})} \tag{5.16}$$

and describes the probability that the fit yields a χ^2 value exceeding the measured value in a fit with $\mathcal{N}$ degrees of freedom. The resulting distribution of $P_{\chi^2}(\mathcal{N})$ should be evenly spread between 0 and 1 if the error estimates used in the calculation of χ^2 are correct and Gaussian and the events are reconstructed properly. The expectation value of $\frac{\chi^2}{\mathcal{N}}$ is unity. An example for the fit probability can be found in chapter 6.1.3, figure 6.4.

Chapter 6

Treatment of Invariant W Boson Mass Spectra

A standard method used in the measurement of the W boson mass is the unbinned likelihood fit, a method, where the likelihood for each event is given by a *probability density function* or *physics function* $f(m; M_W, \Gamma_W, \sqrt{s})$. The function is evaluated at the reconstructed event mass m and depends on the mass and width of the W boson and the center-of-mass energy $\sqrt{s}$. The physics function is expected to be the best estimate of the reconstructed event mass distribution. To extract the W boson mass M_W from a whole sample of data, the total likelihood — given by the product of the individual event likelihoods — is maximized. But this method only works well as long as the errors of the individual events are in the same energy region. The problem with the semileptonic channel is the fact that the measurement errors vary from event to event due to the unknown amount of energy carried away by the undetected neutrino. The analysis of $W^+W^- \to \mathrm{q\bar{q}}l\bar{\nu}_l$ events therefore calls for another approach that is made by the *convolution fit*, a method based on the unbinned likelihood fit, that takes the individual measurement errors into account. The general method of the convolution fit will be described in 6.1. The second section (chapter 6.2) deals with a method to locate possible biases in the mass measurement. Statistical errors are estimated from the analysis of data sized Monte Carlo samples and the systematic uncertainties in the measurement of the mass of the W boson are determined in the following (chapter 6.3). The results obtained from the application of the convolution fit on 1999 and 2000 data ($\sqrt{s}$ = 192 – 206.5 GeV) will be presented in chapter 6.4.

6.1 Analysis Method: The Convolution Fit

The convolution fit uses the information of each single event in an unbinned likelihood fit of a theoretical distribution to a data sample. For each event, the *event probability density* or *error density* $P_i(m)$ — the probability that an event originated from a W boson pair with a reconstructed mean W boson mass m — is calculated from the minimization of a χ^2 function (described in further detail in chapter 5.3). The probability that a W boson pair with mean reconstructed mass m is produced in an electron-positron collision for a given W boson mass M_W and width Γ_W is described in the *physics function* $f(m; M_W, \Gamma_W, \sqrt{s})$. In

the next step the event probability density is convolved with the physics function yielding the event likelihood $L_i(M_W, \Gamma_W)$. The total likelihood is given by the product of the individual event likelihoods. A maximum likelihood fit is then applied to obtain the mass of the W boson.

6.1.1 The Event Probability Density

The measurement errors in the semileptonic channel are highly asymmetric. They follow a broad distribution exceeding by far the natural width of the W boson Γ_W that has a value of about 2 GeV. The probability that an event originated from a W boson decay of the mean W boson mass m, the event probability density, is therefore included in the fit procedure. The calculation of the event probability density is based on a kinematic fit using the previously corrected jet and lepton 3-momenta and their covariance matrices as input variables. A kinematic fit usually yields the best estimate of a set of measured and unmeasured parameters by minimizing a χ^2 function. The mass of the W boson is calculated in the following step using the previously calculated best estimates for the jet and lepton momenta. A measure for the goodness-of-fit, the fit probability (equation (5.16)), can be obtained from the value of the χ^2 function. The convolution fit uses a variation of this method. A kinematic fit is applied to obtain the best estimate for a set of parameters *for a given W boson mass m*. The value of $\chi^2(m)$ can be used to calculate a probability describing the likelihood that an event originated from a W boson pair of a given mean mass m. To obtain this probability, the χ^2 function (equation (5.7)) is slightly modified: By adding a fixed mass m another constraint is introduced that has to be considered. This analysis implements a penalty function in the kinematic fit. The additional term can be written as

$$\frac{(m_{12} - m)^2}{\delta_m^2} + \frac{(m_{34} - m)^2}{\delta_m^2} \ , \tag{6.1}$$

replacing the familiar term for the equal mass constraint given in equation (5.7). The resulting $\tilde{\chi}^2$ function,

$$\begin{aligned} \tilde{\chi}^2(m) \quad = \quad & \sum_{ij} (\vec{p}_{meas} - \vec{p})_i \, V_{ij}^{-1} \, (\vec{p}_{meas} - \vec{p})_j + \\ & \frac{(\sum_i E_i - \sqrt{s})^2}{\delta_E^2} + \frac{(m_{12} - m)^2}{\delta_m^2} + \frac{(m_{34} - m)^2}{\delta_m^2} \ , \end{aligned} \tag{6.2}$$

is now minimized with regard to the parameters $\vec{p}$. In this equation, $\vec{p}_{meas}$ and $\vec{p}$ denote the measured and estimated momenta of the jets and the lepton, V^{-1} the inverse covariance matrix, E_i the energy of the i-th jet or lepton and finally $\sqrt{s}$ the center-of-mass energy. m_{12} and m_{34} are the masses of the two W bosons W^+ and W^-. Their values are calculated using equation (5.10).

The event probability density $P_i(m)$ is given by

$$P_i(m) = \frac{1}{N}\, exp\left(-\frac{\tilde{\chi}_i^2(m) - \tilde{\chi}_i^2(m_{ref})}{2}\right) \tag{6.3}$$

where m_{ref} is a reference mass obtained from the minimization of the $\tilde{\chi}^2(m)$. N denotes the normalization factor that is given by

$$N = \int_{-\infty}^{\infty} exp\left(-\frac{\tilde{\chi}_i^2(m) - \tilde{\chi}_i^2(m_{ref})}{2}\right) dm \tag{6.4}$$

Equation (6.3) ensures that a parabolic shape of the χ^2 function yields a Gaussian event probability density. An examples of the χ^2 function and the resulting event probability density is depicted in figure 6.1.

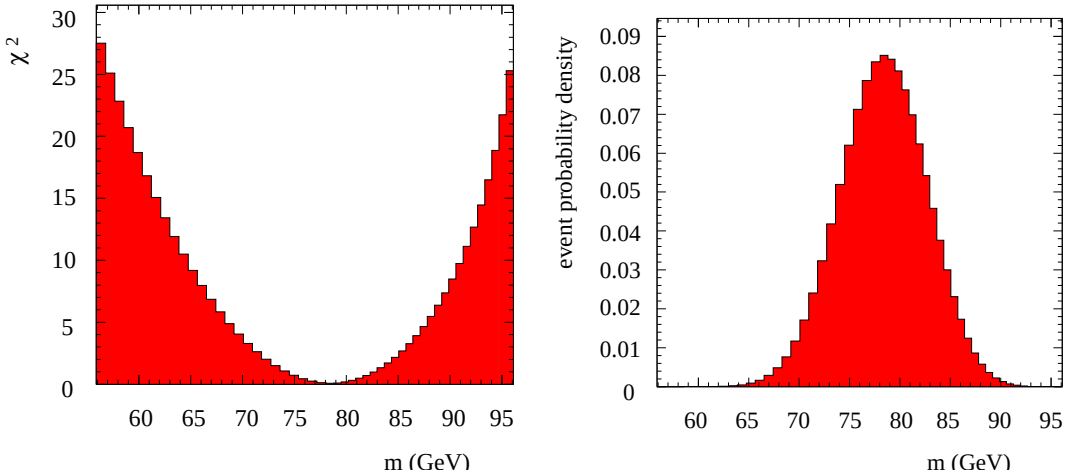

Figure 6.1: *The χ^2 function and the event probability density for a Monte Carlo event generated at a center-of-mass energy of 205 GeV*

6.1.2 The Physics Function

The physics function $f(m; M_W, \Gamma_W, \sqrt{s})$ represents the best estimate of the W boson mass distribution. The function itself is composed of the weighted sum of a signal function $f_{signal}(m; M_W, \Gamma_W, \sqrt{s})$ and several background functions $f_{bg,i}(m)$ for different background sources. Naturally, the signal function depends on the mass M_W and width Γ_W of the W boson and the center-of-mass energy $\sqrt{s}$. Both the signal and the background part of the physics function are described in detail in the section below.

The Signal Part of the Physics Function

The signal part of the physics function is designed to represent the W boson mass distribution one expects for events originating from W boson pair decays. $f_{signal}(m; M_W, \Gamma_W)$

is a superposition of relativistic Breit-Wigner functions $bw(m; M_W, \Gamma_W)$. They are given by

$$bw(m; M_W, \Gamma_W) = \frac{m^2}{(m^2 - M_W^2)^2 + m^2\Gamma_W^2} \cdot \frac{\sqrt{\frac{s}{4} - m^2}}{\frac{\sqrt{s}}{2}} \tag{6.5}$$

The production of W boson pairs stops abruptly at high masses when the maximum available center-of-mass energy is reached. This effect is implemented by the last factor in equation (6.5), the *phase space factor*. It is given by the ratio of the momentum of the W boson p to its amount of energy E. As the mass of both W bosons in a W boson pair is assumed to be equal, the energy of a single W boson amounts to $\sqrt{s}/2$. This result, in combination with equation (5.8), yields the phase space factor in equation (6.5).

Correction of Initial State Radiation Effects

The effects of Initial State Radiation (ISR) have to be considered in the physics function. A photon is thereby emitted by the incoming electron or positron before it reaches the collision point. The two W bosons are thus produced at a lower center-of-mass energy $\sqrt{s'}$. This effect causes a shift of the reconstructed mass towards higher values. This mass shift should not be ignored in the measurement of the W boson mass. As the photon is usually emitted in the direction of the beam pipe — both electron and positron are highly relativistic and thus emit photons preferentially in the forward direction — it escapes unnoticed. Due to the unobserved neutrino, the reconstruction of the photon energy using only the equations of constraints yields a poor resolution. The inclusion of ISR effects in the physics function is therefore based entirely on statistics. To estimate the impact of the mass shift on the W boson mass measurement, we regard the invariant mass of the dijet system. It can be calculated from the 4-momenta of the jets and is given by

$$m = \sqrt{2E_1E_2(1 - cos(\theta))} \tag{6.6}$$

where E_1 and E_2 denote the energies of the two jets and θ the angle between them. The masses of the jets are neglected. A scaling factor to the total energy of the W boson is introduced to ensure energy conservation and the fulfillment of the equal mass constraint. The energy of each W boson now amounts to the beam energy ($\sqrt{s}/2$). The total energies of the jets, E_1 and E_2, are changed accordingly:

$$\begin{aligned} E_1 &\to E_1 \frac{\sqrt{s}/2}{E_1 + E_2} \\ E_2 &\to E_2 \frac{\sqrt{s}/2}{E_1 + E_2} \end{aligned} \tag{6.7}$$

Naturally, the mass of the dijet system has to be changed as well:

$$m \rightarrow \sqrt{2E_1E_2(\frac{\sqrt{s}/2}{E_1+E_2})^2(1-cos(\theta))} \tag{6.8}$$

Equation (6.8) can be used to estimate the correction needed in the treatment of Initial State Radiation effects. Due to the emission of a photon, the event is produced at a reduced center-of-mass $\sqrt{s'}$. In analogy to equation (6.8) the mass of the system can be written as

$$m' = \sqrt{2E_1E_2(\frac{\sqrt{s'}/2}{E_1+E_2})^2(1-cos(\theta))} \tag{6.9}$$

The reconstructed mass is determined at the nominal center-of-mass energy $\sqrt{s}$. A comparison between equation (6.8) and (6.9) shows that the real mass of the W boson can be calculated using the reconstructed mass m:

$$m' = m\sqrt{\frac{s'}{s}} \tag{6.10}$$

The mass shift in the reconstructed mass is thus given by

$$\Delta m = m - m' = (\sqrt{s} - \sqrt{s'})\frac{m}{\sqrt{s}} \tag{6.11}$$

To compensate for this effect the reconstructed mass is reduced accordingly. The corrected mass can be written as

$$m_{corr} = m - (\sqrt{s} - \sqrt{s'})\frac{m}{\sqrt{s}} \tag{6.12}$$

As the actual center-of-mass energy at the collision point cannot be determined, another factor Q(s') is needed to describe the probability that an event was actually produced at a reduced center-of-mass energy $\sqrt{s'}$. This factor is obtained from Monte Carlo studies and included in the physics function. We thus obtain the ISR corrected signal function:

$$f_{signal}(m; M_W, \Gamma_W) = \frac{1}{N}\int_0^s bw(m_{corr}; M_W, \Gamma_W) \times Q(s')ds' \tag{6.13}$$

where N denotes the normalisation factor of the signal function. A comparison between the signal function $f_{signal}(m; M_W, \Gamma_W)$ and a relativistic Breit-Wigner function is depicted in figure 6.2. The Breit-Wigner function includes a phase space factor.

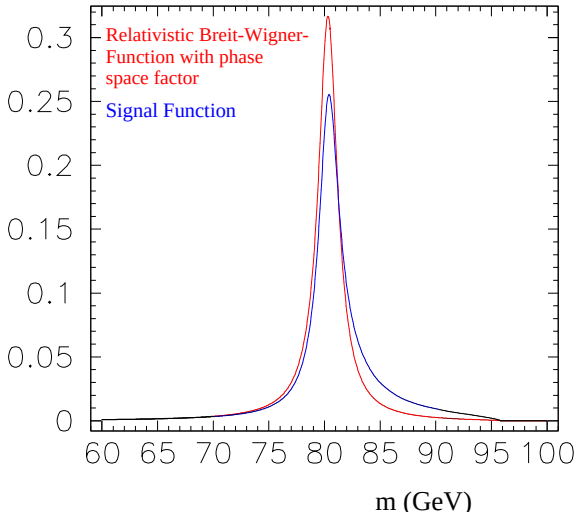

Figure 6.2: *Comparison between the signal function and a relativistic Breit-Wigner function including a phase space factor. The functions are created at a center-of-mass energy of 192 GeV.*

The Background Part of the Physics Function

The background part of the physics function consists of several separate functions describing the mass distributions of the most important background processes. Their shape and the mean number of events contained in each background function are taken from Monte Carlo distributions of the corresponding background source. The following processes are considered in this analysis:

- $e^+e^- \rightarrow Z^0/\gamma \rightarrow \mathrm{q\bar{q}}$
- 4 fermion WW final states
- 4 fermion non-WW final states
- evil tau background

Evil tau events are events for which the reconstructed tau direction deviates more than 15 degree from the true tau direction. Details on the 4 fermion background effects can be found in chapter 2.3. The mass distributions of different background processes are depicted in figure 6.3.

The different background functions, their shape and mean number of events, are determined by applying the same selections and cuts on Monte Carlo background samples as on data samples. The number of events thus obtained for each background process is scaled to the integrated data luminosity. A kinematic fit (a 2C-fit for the $\mathrm{q\bar{q}}e\bar{\nu}_e$ and $\mathrm{q\bar{q}}\mu\bar{\nu}_\mu$ channel and a 1C-fit for the $\mathrm{q\bar{q}}\tau\bar{\nu}_\tau$ channel) yields the mass distribution of the different background processes and thus the shapes of the background functions $f_{bg,i}(m)$. The background part of the physics function can be written as a weighted sum of these functions.

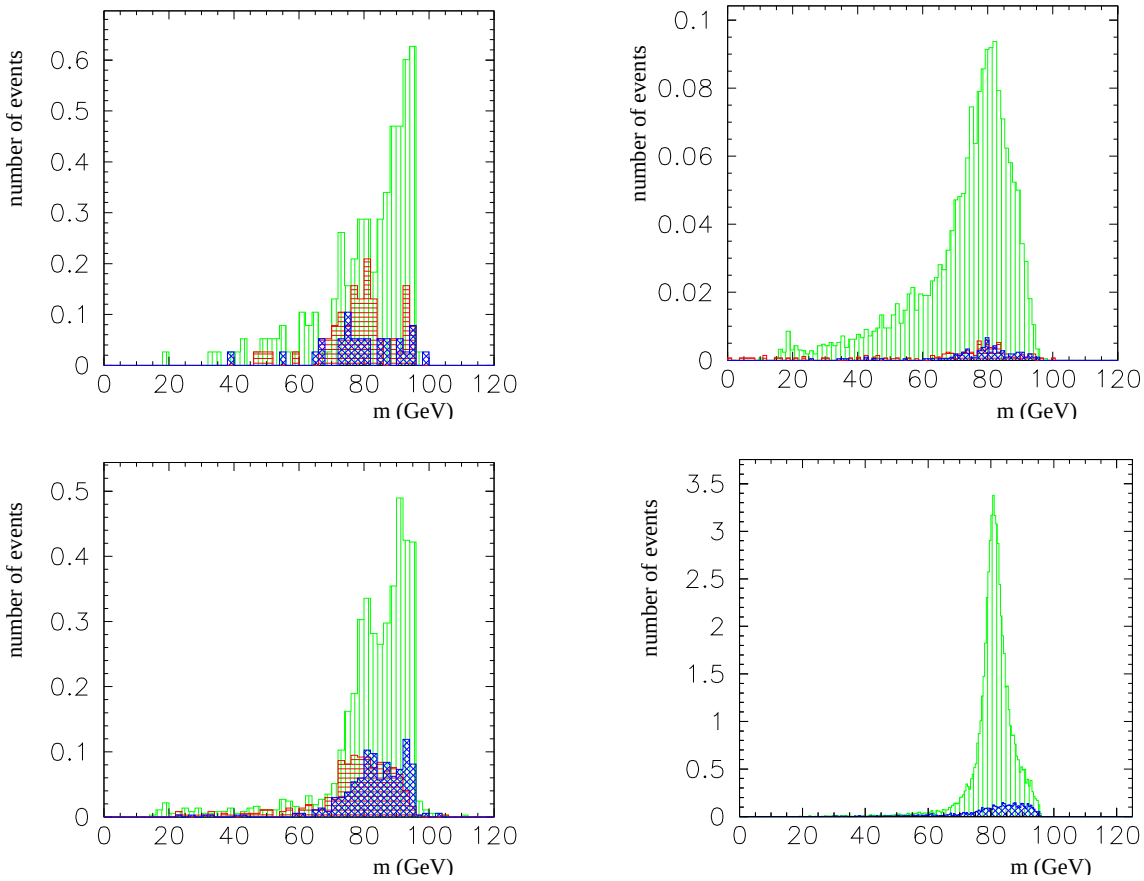

Figure 6.3: *Background shapes included in the physics function. The depicted background processes are:* $Z^0/\gamma \rightarrow q\bar{q}$ *background (top left), four-fermion WW final states background (top right) and four-fermion non-WW final states (bottom left). The different semileptonic channels are presented in different colours (red:* $q\bar{q}e\bar{\nu}_e$*, blue:* $q\bar{q}\mu\bar{\nu}_\mu$ *and green:* $q\bar{q}\tau\bar{\nu}_\tau$*). All three plots use a bin width of 5 GeV. The last plot (bottom right) shows the evil tau background shape (blue) in comparison with a* $W^+W^- \rightarrow q\bar{q}\tau\bar{\nu}_\tau$ *mass distribution (green). It uses a bin width of 1 GeV. All events are generated at a center-of-mass energy of* $\sqrt{s}$*=192 GeV*

A combination of the signal and the background part yields the complete physics function:

$$f(m; M_W, \Gamma_W, \sqrt{s}) = \left(1 - \sum_i \frac{< N_{bg,i} >}{< N_{total} >}\right) f_{signal}(m; M_W, \Gamma_W, \sqrt{s}) + \sum_i \frac{< N_{bg,i} >}{< N_{total} >} f_{bg,i}(m) \quad (6.14)$$

In this equation, $< N_{total} >$ denotes the mean total number of expected events, $< N_{bg,i} >$ the mean number of background events and $f_{bg,i}(m)$ the mass distributions of the contributing background processes.

6.1.3 Cuts on Kinematic Fit Properties

All events passing the previous selections described in chapter 5.1 are now subjected to another set of cuts. Three further cuts are applied to kinematic fit properties. One cut is made on the fit probability $P_{\chi^2}(m_{ref})$ (equation (5.16)) as this parameter is a measure for the goodness-of-fit. m_{ref} denotes the reference mass obtained from the minimization of the χ^2 function. Two further cuts are applied to the χ^2 function for more technical reasons. The cuts are given by

- $P_{\chi 2}(m_{ref}) > 10^{-3}$
- smoothness of the χ^2 function
- $\Delta\chi^2 = \chi^2(m_{a,b}) - \chi^2(m_{ref}) \geq 25$

As already explained in chapter 5.3.3, the fit probability can be used to exclude badly reconstructed events that passed the semileptonic event selection. $P_{\chi 2}(m_{ref})$ denotes the value of the fit probability at the absolute minimum of the χ^2 function, m_{ref} the mass at this point. An example for the fit probability is depicted in figure 6.4. The peak close to zero originates mainly from events where the fit failed. They are excluded by the first cut.

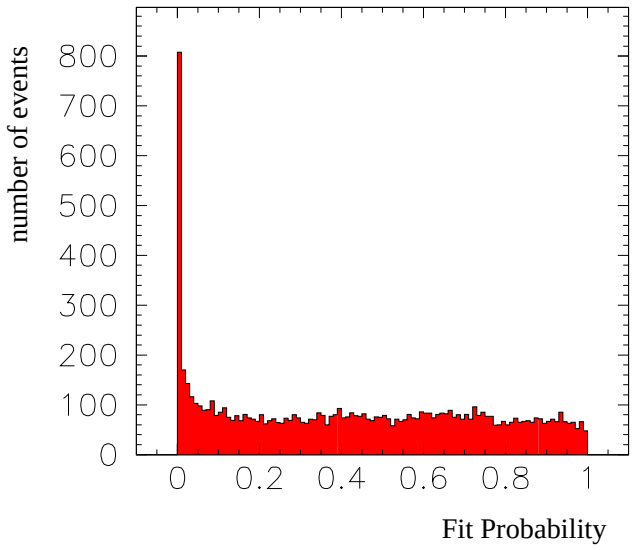

Figure 6.4: *Fit probability of a Monte Carlo sample generated at a center-of-mass energy of* $\sqrt{s}$*=192 GeV. A cut on the fit probability is applied to remove badly reconstructed events.*

The two cuts on the χ^2 function are used to remove events for which the calculation of the event probability density failed for technical reasons. The first cut demands the smoothness of the χ^2 function, as points of discontinuity indicate failures in the fit. The second cut ensures that a mass range of 5 σ is given on both sides of m_{ref}. This mass range is needed to allow a proper normalisation of the event probability density.

6.1.4 The Maximum Likelihood Fit

Now that the physics function is constructed and the event probability density is calculated, a maximum likelihood fit is applied to obtain the desired mass of the W boson. A maximum likelihood fit compares data to a theoretical *parent distribution*, varying the different parameters until the likelihood — the probability that the observed data sample originates from this parent distribution — reaches its maximum. In doing so, the likelihood of each single event is taken into consideration. For uncorrelated data the total likelihood is given by the product of the different event likelihoods. In the convolution fit the convolution of the event probability density $P_i(m)$ and the physics function $f(m; M_W, \Gamma_W, \sqrt{s})$ yields the *event likelihood* $L_i(M_W, \Gamma_W)$,

$$L_i(M_W, \Gamma_W) = \int_0^\infty f(m; M_W, \Gamma_W, \sqrt{s})\, P_i(m)\, dm \ . \tag{6.15}$$

As the contributing events are independent measurements, the total likelihood $\mathcal{L}(M_W, \Gamma_W)$ is calculated as the product of the individual event likelihoods:

$$\mathcal{L}(M_W, \Gamma_W) = \prod_{i=1}^{N} L_i(M_W, \Gamma_W) \ . \tag{6.16}$$

N denotes the number of events in the data sample.

The maximisation of the total likelihood yields the mass of the W boson. For the numerical calculation it is more convenient to maximize the logarithm of the total likelihood instead. This method is used in this analysis to avoid computational problems. The measurements are carried out separately for each semileptonic decay channel. A combined result is obtained by minimizing a variation of the χ^2 function:

$$\chi^2 = (M_{W,i} - M_W)\, C^{-1}\, (M_{W,i} - M_W) \tag{6.17}$$

where $M_{W,i}$ are the W boson masses measured in the different decay channels ($q\bar{q}e\bar{\nu}_e$, $q\bar{q}\mu\bar{\nu}_\mu$ and $q\bar{q}\tau\bar{\nu}_\tau$), M_W is the combined result for all channels and C^{-1} is the inverse covariance matrix consisting of both statistical and systematic errors obtained from all measurements. The covariance matrix can be written as

$$C = C_{stat} + \sum C_{syst} \tag{6.18}$$

where C_{stat} is a diagonal matrix, its elements are given by the squared statistical errors. C_{syst} contains information about systematic errors. In the case of uncorrelated systematic errors the corresponding covariance matrices are diagonal and the entries are the squared errors. They contain off-diagonal elements if the systematic errors are correlated. These off-diagonal elements are then given by the product of the correlation coefficient and

the errors in the corresponding channels. This method takes the correlations between systematic errors correctly into account but unfortunately the clear distinction between statistical and systematic errors thus gets lost. The analysis only yields a total error, the separate values of the systematic errors are later retrieved using the following relation

$$\sigma^2_{total} = \sigma^2_{stat} + \sigma^2_{syst} \tag{6.19}$$

6.2 Ensemble Tests

In ensemble tests the analysis method, in this case the convolution fit, is applied to an ensemble of data sized Monte Carlo experiments. Statistical methods can be used to interpret the results and locate possible biases in the mass measurement that are taken into account in the analysis of real data.

6.2.1 General Method

An ensemble of Monte Carlo samples is constructed in the following way: The data sample is analysed to determine the number of selected events in each of the three semileptonic decay channels. The same number of $q\bar{q}e\bar{\nu}_e$, $q\bar{q}\mu\bar{\nu}_\mu$ and $q\bar{q}\tau\bar{\nu}_\tau$ events as selected from data is included in each Monte Carlo sample. The mean number of background events and the mass distribution for Z^0/γ and four-fermion final states background are determined by applying the same cuts and selections on Monte Carlo background samples as on real data. The resulting number of background events has to be scaled to the integrated data luminosity. The background events included in each sample are chosen randomly from a Poisson distribution with a mean value identical to the mean number of background events thus obtained. To reduce possible correlations, the events are only used once. If the number of selected background events exceeds the number of available Monte Carlo events a randomly chosen event and the subsequent events are reused. After the determination of the number of background events the rest of the sample is filled with signal Monte Carlo events naturally including evil tau background events. Now that the ensemble is constructed, each sample is subjected to the convolution fit. We thus obtain an individual value for the mass of the W boson from each sample. A Gaussian fit to the resulting mass distribution provides the fitted W boson mass and the corresponding statistical error.

6.2.2 The Calibration Function

There are various effects that might cause a bias in the mass measurement of the W boson. The correction of Initial State Radiation, for example, is based on a single Monte Carlo simulation for a W boson mass of 80.33 GeV at each center-of-mass energy and some of the four-fermion final states background effects included in the physics function depend on the mass of the W boson, to mention at least some of the effects resulting in a possible bias in the measurement of the W boson mass. To compensate for this bias, ensemble tests are made for Monte Carlo samples with five different input masses M_{true}: 79.83 GeV, 80.08 GeV, 80.33 GeV, 80.58 GeV and 80.83 GeV. The application of the convolution fit

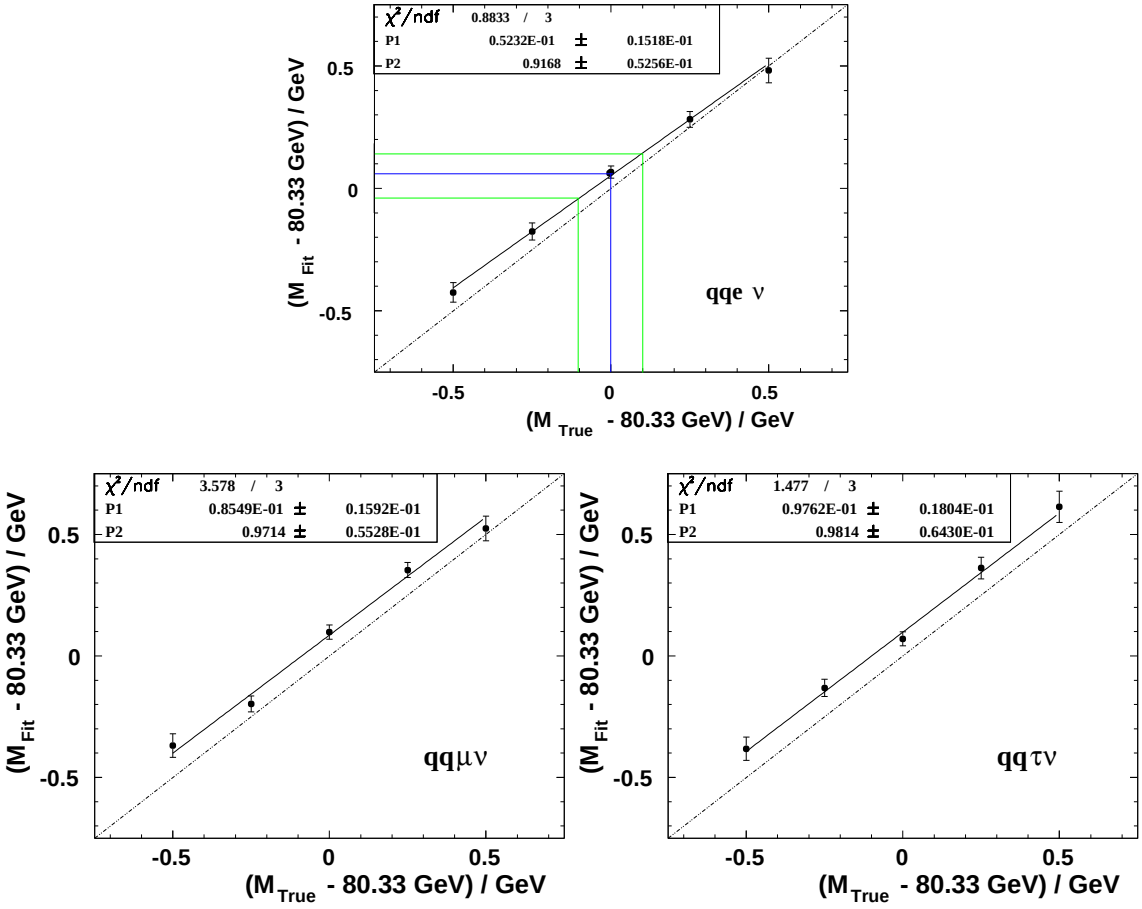

Figure 6.5: *Calibration functions for the measurement of the W boson mass generated at a center-of-mass energy of $\sqrt{s}$=200 GeV. All semileptonic decay channels are represented.*

to each ensemble of Monte Carlo samples yields the mean reconstructed mass M_{fit} and the corresponding error. A straight line fit (M_{true} against M_{fit}) is now used to obtain a calibration function for the measurement of the W boson mass. The calibration function is given by

$$(M_{fit} - 80.33\ GeV) = \alpha + \beta\ (M_{true} - 80.33\ GeV) \tag{6.20}$$

Equation (6.20) directly yields a correction for bias effects in the mass measurement:

$$M_{true} = \frac{M_{fit} - \alpha}{\beta} + 80.33\ GeV\ (1 - \frac{1}{\beta}) \tag{6.21}$$

Examples for the calibration functions in the different semileptonic decay channels are depicted in figure 6.5. Slope and offset of the calibration functions for center-of-mass energies between 192 and 206.5 GeV are listed in table 6.1.

The calibration function also yields a correction factor for the statistical errors: The slope β of the calibration function is expected to be consistent with unity. Smaller values

$\sqrt{s} = 192\ GeV$			$\sqrt{s} = 196\ GeV$		
channel	slope $\beta \pm \delta\beta$	offset $\alpha \pm \delta\alpha$	channel	slope $\beta \pm \delta\beta$	offset $\alpha \pm \delta\alpha$
$q\bar{q}e\bar{\nu}_e$	0.957 ± 0.061	0.055 ± 0.016	$q\bar{q}e\bar{\nu}_e$	0.982 ± 0.051	0.094 ± 0.015
$q\bar{q}\mu\bar{\nu}_\mu$	1.045 ± 0.052	0.052 ± 0.015	$q\bar{q}\mu\bar{\nu}_\mu$	1.023 ± 0.051	0.095 ± 0.015
$q\bar{q}\tau\bar{\nu}_\tau$	1.000 ± 0.066	-0.009 ± 0.018	$q\bar{q}\tau\bar{\nu}_\tau$	0.890 ± 0.069	0.075 ± 0.019
$\sqrt{s} = 200\ GeV$			$\sqrt{s} = 202\ GeV$		
channel	slope $\beta \pm \delta\beta$	offset $\alpha \pm \delta\alpha$	channel	slope $\beta \pm \delta\beta$	offset $\alpha \pm \delta\alpha$
$q\bar{q}e\bar{\nu}_e$	0.917 ± 0.053	0.052 ± 0.015	$q\bar{q}e\bar{\nu}_e$	1.072 ± 0.057	0.082 ± 0.017
$q\bar{q}\mu\bar{\nu}_\mu$	0.971 ± 0.055	0.085 ± 0.016	$q\bar{q}\mu\bar{\nu}_\mu$	0.908 ± 0.055	0.092 ± 0.016
$q\bar{q}\tau\bar{\nu}_\tau$	0.981 ± 0.064	0.098 ± 0.018	$q\bar{q}\tau\bar{\nu}_\tau$	0.905 ± 0.067	0.156 ± 0.019
$\sqrt{s} = 205\ GeV$			$\sqrt{s} = 206.5\ GeV$		
channel	slope $\beta \pm \delta\beta$	offset $\alpha \pm \delta\alpha$	channel	slope $\beta \pm \delta\beta$	offset $\alpha \pm \delta\alpha$
$q\bar{q}e\bar{\nu}_e$	1.057 ± 0.055	0.046 ± 0.016	$q\bar{q}e\bar{\nu}_e$	1.000 ± 0.043	0.065 ± 0.014
$q\bar{q}\mu\bar{\nu}_\mu$	1.002 ± 0.063	0.065 ± 0.017	$q\bar{q}\mu\bar{\nu}_\mu$	0.973 ± 0.062	0.093 ± 0.017
$q\bar{q}\tau\bar{\nu}_\tau$	0.890 ± 0.084	0.068 ± 0.021	$q\bar{q}\tau\bar{\nu}_\tau$	0.976 ± 0.067	0.102 ± 0.020

Table 6.1: *Slope and offset of the various calibration functions for center-of-mass energies between 192 and 206.5 GeV in the three semileptonic decay channels. They are used in this analysis to correct for bias effects in the mass measurement.*

of β lead to an underestimation of the statistical errors obtained from the maximum likelihood fit as a certain mass range around M_{true} on the x-axis (denoted by the green lines on both sides of $M_{true} = 80.33\ GeV$ in figure 6.5) is reduced in size when it is reproduced on the y-axis. Larger values of β respectively result in an overestimation of the statistical error. This effect is compensated for by the application of a correction factor $1/\beta$ to the statistical errors.

6.2.3 The Pull Distribution

Another quantity that can be used to detect possible errors or deviations in the measurement of the mass of the W boson is the *Pull Distribution*.

The Pull Distribution is defined as

$$P = \frac{M_{fit} - M_{true}}{\sigma_{fit}} \tag{6.22}$$

where M_{fit} denotes the mass value obtained from the maximum likelihood fit, M_{true} the input mass of the Monte Carlo samples and σ_{fit} the measurement error. If the fit is carried out correctly with only statistical fluctuations in the mass measurement, the Pull Distribution is expected to have a Gaussian shape centered around zero and a pull width consistent with unity. Systematic shifts in the mass measurement result in a dislocation

of the Pull Distribution, incorrect determinations of the individual measurement errors lead to a deviation of the pull width from unity. Deviations of the Pull Distribution from the Gaussian shape indicate inherent errors in the fit procedure, they cannot be explained by mere statistical fluctuations. The correction of systematic shifts is already carried out using equation (6.21), but the width of the Pull Distribution yields a correction factor for miscalculated statistical errors.

As the Pull Distribution is defined by the deviation of the measured mass value M_{fit} from the input mass M_{true} divided by the measurement error, a pull width exceeding unity indicates an underestimation of the statistical errors, a smaller value respectively an overestimation. A second correction factor σ is therefore applied, the width of the Pull Distribution. We thus obtain a scaling factor for statistical errors:

$$\frac{\sigma}{\beta} \qquad \left(\frac{pull\,width}{slope\,of\,the\,calibration\,function} \right)$$

The slopes of the different calibration functions for all channels and energies between 192 and 206.5 GeV are listed in table 6.1. Table 6.2 provides the widths of the different pull distributions. A typical example of a Pull Distribution obtained from ensemble tests is shown in figure 6.6.

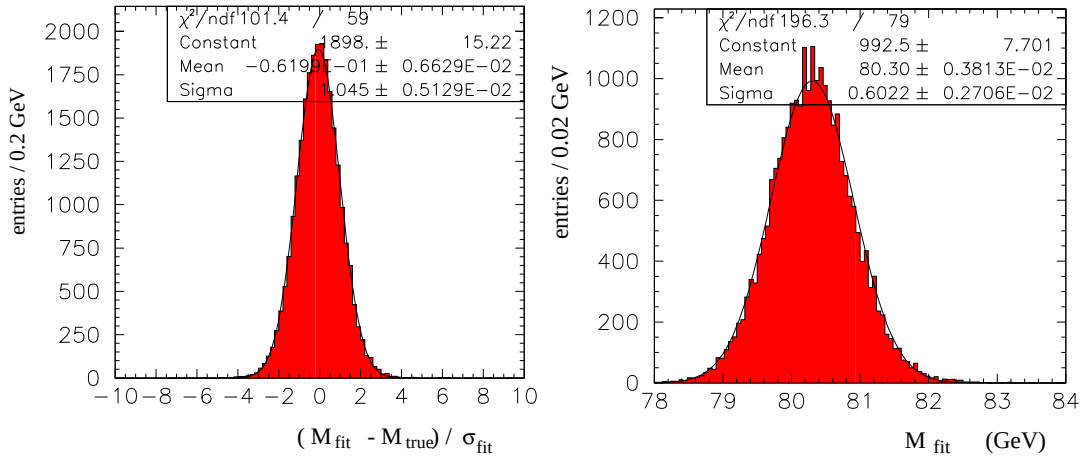

Figure 6.6: *Pull Distribution obtained from ensemble tests and corresponding mass distribution of the W boson for a center-of-mass energy of* $\sqrt{s}$*=192 GeV. The* $q\bar{q}\tau\bar{\nu}_\tau$ *channel is depicted in this figure.*

$\sqrt{s}$ = 192 *GeV*		$\sqrt{s}$ = 196 *GeV*	
channel	pull width	channel	pull width
$q\bar{q}e\bar{\nu}_e$	1.051 ± 0.006	$q\bar{q}e\bar{\nu}_e$	1.057 ± 0.006
$q\bar{q}\mu\bar{\nu}_\mu$	1.007 ± 0.005	$q\bar{q}\mu\bar{\nu}_\mu$	1.002 ± 0.006
$q\bar{q}\tau\bar{\nu}_\tau$	1.045 ± 0.005	$q\bar{q}\tau\bar{\nu}_\tau$	1.000 ± 0.007
$\sqrt{s}$ = 200 *GeV*		$\sqrt{s}$ = 202 *GeV*	
channel	pull width	channel	pull width
$q\bar{q}e\bar{\nu}_e$	1.037 ± 0.005	$q\bar{q}e\bar{\nu}_e$	1.080 ± 0.005
$q\bar{q}\mu\bar{\nu}_\mu$	1.012 ± 0.005	$q\bar{q}\mu\bar{\nu}_\mu$	1.023 ± 0.005
$q\bar{q}\tau\bar{\nu}_\tau$	0.996 ± 0.006	$q\bar{q}\tau\bar{\nu}_\tau$	1.041 ± 0.005
$\sqrt{s}$ = 205 *GeV*		$\sqrt{s}$ = 206.5 *GeV*	
channel	pull width	channel	pull width
$q\bar{q}e\bar{\nu}_e$	1.042 ± 0.005	$q\bar{q}e\bar{\nu}_e$	1.038 ± 0.005
$q\bar{q}\mu\bar{\nu}_\mu$	0.998 ± 0.005	$q\bar{q}\mu\bar{\nu}_\mu$	0.994 ± 0.005
$q\bar{q}\tau\bar{\nu}_\tau$	1.028 ± 0.005	$q\bar{q}\tau\bar{\nu}_\tau$	1.007 ± 0.005

Table 6.2: *Widths of various pull distributions obtained from ensemble tests for all semileptonic decay channels and energies between 192 and 206.5 GeV. They are used as scaling factors in the correction of misestimated statistical errors.*

6.3 Expected Errors

6.3.1 Statistical Errors

For the estimation of statistical errors this analysis uses a method already introduced in chapter 6.2. An ensemble of Monte Carlo samples is created including the same number of $q\bar{q}e\bar{\nu}_e$, $q\bar{q}\mu\bar{\nu}_\mu$ and $q\bar{q}\tau\bar{\nu}_\tau$ events as selected from data including a certain number of background events. The convolution fit, applied to the different samples, yields a fitted W boson mass and a corresponding error. The estimated statistical error one has to expect in the analysis is given by the width of the resulting mass distribution. To get high statistical precision, up to 25000 samples are included in the analysed ensemble. In the previous two chapters methods were explained that are used to locate possible errors or deviations in the determination of the fitted mass. One of the two correction factors used in the compensation of possible measurement biases has to be used in the calculation of the expected statistical error as well: The slope of the calibration function. As already explained in chapter 6.2.2 the statistical errors are overestimated, if the slope of the calibration function exceeds a value of one and respectively underestimated for smaller values. A scaling factor of $1/\beta$ is therefore applied to the expected statistical errors. The second scaling factor explained above, the width of the Pull Distribution, is only applied to data errors. The *expected* statistical errors are obtained from ensemble tests that do not take the individual measurement error into account. It is therefore not necessary to scale the expected statistical error with the pull width σ. We thus obtain a scaling factor for expected statistical errors of $1/\beta$.

The slopes of the different calibration functions for all channels and energies between 192 and 206.5 *GeV* along with both the corrected and uncorrected expected statistical

errors are listed in table 6.3.

6.3.2 Systematic Errors

There are many effects leading to systematic uncertainties in the measurement of the W boson mass. The influence of other measurements on the parameters used in this analysis has to be considered along with errors caused by finite statistics or incomplete models of the Monte Carlo samples included in the physics function. The impact of these effects on the mass measurement is studied with ensemble tests as well. An ensemble of Monte Carlo samples, the *systematic ensemble*, is corrected with regard to one effect and compared to a so called *reference ensemble* that is left unchanged. The bias of the mass measurement is determined using the following calculation:

For an ensembles consisting of N Monte Carlo samples the mean mass of the W boson $\langle M_W \rangle$ is given by

$$\langle M_W \rangle \;=\; \frac{1}{N} \sum_{i=1}^{N} M_i \tag{6.23}$$

where M_i denotes the mass obtained from the i-th Monte Carlo sample. The bias ΔM_W is the difference between the mean masses of both ensembles:

$$\Delta M_W \;=\; \langle M_{syst} \rangle - \langle M_{ref} \rangle \tag{6.24}$$

It is also possible to analyse correlations between the systematic and the reference ensemble. A *correlation coefficient* ρ is defined as a measure for these correlations. ρ yields a value of 0 for uncorrelated systematic uncertainties and a value of 1 if they are fully correlated. The correlation coefficient is given by

$$\rho \;=\; \frac{1}{N-1} \sum_{i=1}^{N} \frac{(M_{syst,i} - \langle M_{syst} \rangle)\;(M_{ref,i} - \langle M_{ref} \rangle)}{\delta\langle M_{syst} \rangle \;\; \delta\langle M_{ref} \rangle} \tag{6.25}$$

Again, N denotes the number of Monte Carlo samples included in each ensemble, $M_{syst,i}$ and $M_{ref,i}$ are the W boson masses obtained from the i-th sample of the systematic and the reference ensemble. $\langle M_{syst} \rangle$ and $\langle M_{ref} \rangle$ are the corresponding mean W boson masses of the whole ensemble. The error $\delta\langle M \rangle$ of the mean W boson mass is given by

$$(\delta\langle M \rangle)^2 = \frac{1}{N\,(N-1)} \sum_{i=1}^{N} (M_i - \langle M \rangle)^2 \tag{6.26}$$

$\sqrt{s} = 192\ GeV \quad (\int Ldt = 29.0\,pb^{-1})$			
channel	expected error	β	corrected error
$q\bar{q}e\bar{\nu}_e$	443	0.957	463
$q\bar{q}\mu\bar{\nu}_\mu$	495	1.045	474
$q\bar{q}\tau\bar{\nu}_\tau$	602	1.000	602
combined	289		290
$\sqrt{s} = 196\ GeV \quad (\int Ldt = 77.0\,pb^{-1})$			
channel	expected error	β	corrected error
$q\bar{q}e\bar{\nu}_e$	266	0.982	271
$q\bar{q}\mu\bar{\nu}_\mu$	289	1.023	283
$q\bar{q}\tau\bar{\nu}_\tau$	333	0.890	374
combined	169		173
$\sqrt{s} = 200\ GeV \quad (\int Ldt = 74.0\,pb^{-1})$			
channel	expected error	β	corrected error
$q\bar{q}e\bar{\nu}_e$	297	0.917	324
$q\bar{q}\mu\bar{\nu}_\mu$	312	0.971	321
$q\bar{q}\tau\bar{\nu}_\tau$	342	0.981	349
combined	182		191
$\sqrt{s} = 202\ GeV \quad (\int Ldt = 37.0\,pb^{-1})$			
channel	expected error	β	corrected error
$q\bar{q}e\bar{\nu}_e$	386	1.072	360
$q\bar{q}\mu\bar{\nu}_\mu$	473	0.908	521
$q\bar{q}\tau\bar{\nu}_\tau$	534	0.905	590
combined	261		265
$\sqrt{s} = 205\ GeV \quad (\int Ldt = 83.0\,pb^{-1})$			
channel	expected error	β	corrected error
$q\bar{q}e\bar{\nu}_e$	302	1.057	286
$q\bar{q}\mu\bar{\nu}_\mu$	319	1.002	318
$q\bar{q}\tau\bar{\nu}_\tau$	403	0.890	453
combined	193		192
$\sqrt{s} = 206.5\ GeV \quad (\int Ldt = 137.6\,pb^{-1})$			
channel	expected error	β	corrected error
$q\bar{q}e\bar{\nu}_e$	235	1.000	235
$q\bar{q}\mu\bar{\nu}_\mu$	242	0.973	249
$q\bar{q}\tau\bar{\nu}_\tau$	278	0.976	285
combined	144		147

Table 6.3: *Expected statistical errors in MeV for energies between 192 and 206.5 GeV with and without the application of the correction factor* $1/\beta$ *(1/slope of the calibration function).*

The error on the bias ΔM_W can be calculated using the individual errors of the mean W boson masses of both ensembles and an additional factor that takes the correlations between them into account:

$$(\delta\Delta M_W)^2 = (\delta\langle M_{syst}\rangle)^2 + (\delta\langle M_{ref}\rangle)^2 - 2\,\rho\,\delta\,\langle M_{syst}\rangle\langle M_{ref}\rangle \tag{6.27}$$

The systematic error δ_{syst} of the mass measurement is given by the bias ΔM_W (equation (6.24)), if this bias exceeds the standard deviation σ. If the bias is consistent with zero within the 1 σ interval, the error on the bias (equation (6.27)) is taken as the value of δ_{syst}.

The ensemble tests are carried out separately for each of the three semileptonic decay channels. The resulting systematic errors are then combined in a weighted average, using the statistical errors of the data sample and the systematic errors of the corresponding channel as weights:

$$\bar{\delta} = \sum_i \frac{\delta_i}{\sigma^2_{syst,i} + \sigma^2_{stat,i}} \tag{6.28}$$

When it comes to the combination of the different decay channels, one has to differentiate between correlated and uncorrelated systematic errors. The systematic error of uncorrelated sources is determined by calculating the weighted average $\bar{\delta}$ for both the systematic and the reference sample separately for each decay channel. A comparison between the values obtained from the systematic and the reference sample yields a bias and thus a systematic error for each channel. The individual errors are now added quadratically. For correlated sources the errors of all decay channels are combined in a weighted average using equation 6.28 before the bias is calculated. This bias yields the combined systematic error.

This analysis includes studies on the following systematic error sources:

Beam Energy

For 1999 data ($\sqrt{s} = 192 - 202\,GeV$) the beam energy is known with a precision of 21 GeV [27], for 2000 data ($\sqrt{s} = 205 - 206.5\,GeV$) with a precision of 25 GeV [27]. To estimate systematic errors caused by inaccuracies in the value of the beam energy, the value of the beam energy precision is added to the beam energy in the systematic ensemble.

Error on the Bias Correction

The systematic error inherent in the bias correction is caused by the limited number of available Monte Carlo samples used in the ensemble tests. The resulting error on the bias correction (equation (6.20)) can be written as

$$\delta^2_{bias} = \left(\frac{\delta\alpha}{\beta}\right)^2 + \left(\frac{M_{fit} - 80.33\ GeV - \alpha}{\beta^2}\,\delta\beta\right)^2 \tag{6.29}$$

In this equation, α and β denote slope and offset of the calibration function, $\delta\alpha$ and $\delta\beta$ the corresponding errors and M_{fit} the measured mass of the W boson.

Initial State Radiation

The systematic error associated with uncertainties in the modelling of Initial State Radiation is estimated by comparing a KoralW Monte Carlo sample using a $0(\alpha^3)$ treatment of Initial State Radiation (reference ensemble) to a sample, where the event likelihoods are reweighted to correspond to an $0(\alpha^1)$ treatment (systematic ensemble). In doing so, the KoralW matrix elements for first and third order initial state radiation, $|M_{1st,i}|$ and $|M_{3rd,i}|$, are used as weights:

$$L_i \rightarrow L_i^{|M_{1st,i}|^2/|M_{3rd,i}|^2}$$

Jet and Lepton Energies

The study of systematic errors in the values of the jet and lepton energies takes deviations in the detector calibration and shortcomings in the detector simulation into account. To compensate for discrepancies between data and Monte Carlo, corrections are applied to Monte Carlo events. These corrections are based on a study of Z^0 calibration data compared to Monte Carlo results. This study is implemented in the OPAL WW package [28]. The systematic uncertainties due to jet and lepton energy scales and errors are estimated by varying the correction factors by their uncertainties arising from limited Z^0 data statistics.

Hadronization

For systematic studies on the hadronization model, the model of string fragmentation (chapter 3.2), realized by the multihadron generator JETSET in the reference ensemble, is replaced by the model of cluster fragmentation (chapter 3.2), implemented in the HERWIG generator, in the systematic ensemble. The run numbers of the Monte Carlo samples used in this analysis can be found in appendix A.

Background Effects

Systematic errors in the normalization of Z^0/γ and four-fermion background are caused by uncertainties in the accepted cross sections in the event selection. To estimate these errors, the number of background events in the systematic ensemble is increased accordingly. The cross-sections and the corresponding errors for the center-of-mass energies used in this analysis can be found in [29].

Four Fermion Effects

Studies of the systematic errors associated with four-fermion effects are mainly based on the analysis of interferences between different four fermion diagrams. The event likelihoods L_i obtained from the four-fermion event generator GRC4F (chapter 3.1) are thereby reweighted to correspond to likelihoods obtained from another four-fermion generator, the EXCALIBUR generator. The matrix elements of both generators are used as weights:

$$L_i \rightarrow L_i^{|M_{exc,i}|^2/|M_{grc4f,i}|^2}$$

This method is equivalent to the implementation of EXCALIBUR in the systematic ensemble. As the interferences between different four fermion diagrams are small compared to other effects leading to systematic errors and as the variations of the contributions are small for different center-of-mass energies, the systematic errors used in this analysis are taken from a former analysis on the determination of the W boson mass carried out at $\sqrt{s} = 189\,GeV$ [1].

Fit Procedure

In the estimation of systematic errors inherent in the convolution fit, two changes are made to the fit procedure: The first change is a variation of the mass range around the minimum mass obtained from the χ^2 function in each event. The previously required mass range of at least 5 σ corresponding to a value of $\Delta\chi^2 \geq 25$ is reduced to a mass range of at least 4 σ corresponding to a value of $\Delta\chi^2 \geq 16$. The second change is made with regard to the penalty factors implemented in the kinematic fit. The values of δ_E and δ_m are increased by a factor of 10. As this analysis is the continuation of a former analysis, where the convolution fit was applied to 1997 and 1998 data ($\sqrt{s} = 183\,GeV$ and $\sqrt{s} = 189\,GeV$), and the fit procedure itself is left unchanged, the systematic errors associated with the fit procedure are taken from this former analysis as well [1].

The systematic errors thus obtained for center-of-mass energies between 192 and 206.5 GeV (1999 and 2000) are listed in table 6.4. When combining the measurements of the individual channels, the beam energy, Initial State Radiation, hadronization, jet energy and fit procedure uncertainties are treated as fully correlated. Background, four-fermion, lepton energy and Monte Carlo statistics uncertainties are treated as uncorrelated [30]. Each contribution to the total systematic error is assumed to be independent from the other components and thus added in quadrature to yield the total systematic uncertainty.

	center-of-mass energies					
	192 GeV	196 GeV	200 GeV	202 GeV	205 GeV	206.5 GeV
beam energy	16	16	16	15	16	17
bias correction	24	18	17	15	15	12
Initial State Radiation	1	1	1	1	1	1
jet energy	4	4	3	3	3	3
lepton energy	10	11	13	14	15	13
hadronization	42	53	50	59	42	40
background	20	22	22	25	18	26
four-fermion effects	1	1	1	1	1	1
fit procedure	1	1	1	1	1	1

Table 6.4: *Systematic errors in MeV for center-of-mass energies between 192 and 206.5 GeV. The systematic errors associated with four-fermion effects and with the fit procedure are taken from a former analysis carried out at* $\sqrt{s}$ *=189 GeV (see text for details).*

6.4 Results

The results obtained from the application of the convolution fit to data collected at the OPAL detector in 1999 and 2000 are presented in the following sections. The 1999 data includes the center-of-mass energies 192 GeV, 196 GeV, 200 GeV and 202 GeV. For 2000 data, the analysis is carried out for 205 GeV and 206.5 GeV. The respective results are given in chapter 6.4.1 and chapter 6.4.2. Combined results for all center-of-mass energies between 192 and 206.5 GeV are finally presented in chapter 6.4.3.

6.4.1 Results for 1999 data ($\sqrt{s} = 192 - 202\,GeV$)

The convolution fit described in the previous chapters is now applied to data collected at the OPAL detector in 1999. The different center-of-mass energies are listed in table 6.5 along with the corresponding integrated data luminosities. The event selection is carried out for each of the four center-of-mass energies using the OPAL W group standard routine WW113. Then the cuts on the fit probability and the χ^2 function are applied, yielding the number of selected data events given below. For matters of comparison, the table also contains the number of selected Monte Carlo events scaled to data luminosity. The data results are in good agreement with the expected values.

$\sqrt{s}$	$\int \mathcal{L}\,dt$	data events	Monte Carlo events
192 GeV	29.0 pb^{-1}	152	177
196 GeV	77.0 pb^{-1}	463	439
200 GeV	74.0 pb^{-1}	429	450
202 GeV	37.0 pb^{-1}	228	227

Table 6.5: *Number of selected events for 1999 data compared to the number of selected events obtained from Monte Carlo studies.*

The convolution fit is carried out separately for each of the three semileptonic decay channels. A combined result is calculated later on using equation (6.17). Possible correlations between the systematic errors are taken into account (see chapter 6.1.4 for details). The results of the likelihood fit are corrected for a possible bias in the mass measurement using equation (6.21) and the calibration functions obtained from Monte Carlo studies for each center-of-mass energy. Slope and offset of the individual calibration functions can be found in table 6.1.

The statistical measurement errors are scaled with the inverse slope of the calibration function and the width of the Pull Distribution also obtained from Monte Carlo studies to correct for over- or underestimations. The widths of the Pull Distributions for the different channels and energies can be found in table 6.2.

The results for the fitted mass and the corresponding errors are listed in table 6.6. As already explained in chapter 6.1.4, the analysis method only yields a total error. To allow a better comparison with other measurements, the total error is split into a statistical and a systematic contribution using equation (6.19). The statistical errors prove to be in good agreement with the expected values that are added in parentheses.

$\sqrt{s}$	fitted mass	total error	stat. error	syst. error
192 GeV	80.858	0.278	0.273 (0.290)	0.056
196 GeV	80.881	0.193	0.182 (0.173)	0.064
200 GeV	80.336	0.200	0.190 (0.191)	0.061
202 GeV	80.164	0.266	0.257 (0.265)	0.069

Table 6.6: *Fit results for 1999 data and corresponding errors (in GeV). The values of the expected statistical errors are included in brackets to allow comparison.*

The combined result for all center-of-mass energies is determined by minimizing a χ^2 function (equation (6.17)). The corresponding statistical and systematic errors are included in the covariance matrix (see chapter 6.1.4 for details). A combination of all center-of-mass energies (192-202 GeV) yields the following result for the mass of the W boson in the semileptonic channel:

$$M_W = 80.581 \pm 0.108 \pm 0.056\,GeV$$

with a statistical error of 108 MeV and a systematic error of 56 MeV. The correlations between some of the systematic error sources in the different channels and for different center-of-mass energies accounts for the fact that the combined systematic error of all 1999 data is smaller than the individual systematic errors given in table 6.6.

6.4.2 Results for 2000 data ($\sqrt{s} = 205 - 206.5\,GeV$)

The same procedure is applied to 2000 data. A slight difference to the treatment of 1999 data has to be made with regard to the center-of-mass energies of data events. For 1999 data, the center-of-mass energy is clearly defined. The center-of-mass energy of 2000 data is distributed rather continuously from about 203.5 GeV upwards with distinct peaks in the region of 205 and 206.5 GeV. The corresponding beam energy is depicted in figure 6.7. The collected data is therefore split into two center-of-mass energy regions: All data events with beam energies lower than 102.85 GeV are assigned to the center-of-mass energy of 205 GeV and all data events exceeding this value are assigned to the value of 206.5 GeV up to a beam energy of 103.75 GeV. The analysis of data with beam energies exceeding 103.75 GeV — including the peak at 104 GeV — was delayed as the corresponding Monte Carlo samples needed for the convolution fit are not yet available.

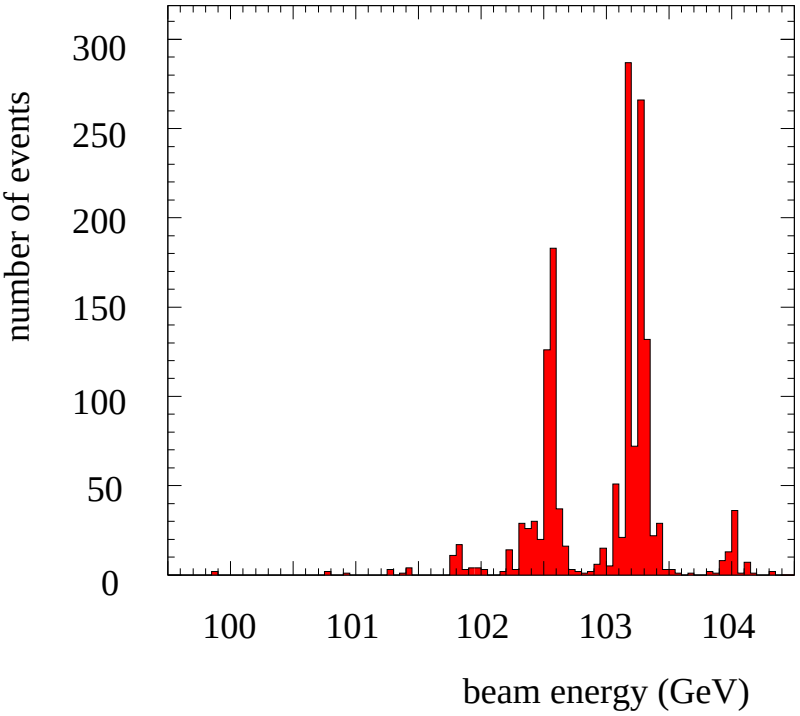

Figure 6.7: *Beam energy of data events collected at the OPAL detector in 2000*

The convolution fit is now carried out as described above in perfect analogy to the analysis of 1999 data. The OPAL package WW114 is used in the event selection, the cuts on χ^2 and on the fit probability remain the same. The number of selected data events, the expected number of events obtained from Monte Carlo studies and the integrated luminosities of the two center-of-mass energies are listed in table 6.7.

The bias corrections (equation (6.21)) are applied to the results of the likelihood fit and the statistical errors are scaled with the width of the Pull Distribution and the inverse slope of the calibration function. The fitted masses obtained from 2000 data and their corresponding errors are given in table 6.8. The separate values for statistical and systematic errors are listed as well to allow a better comparison with alternative methods.

$\sqrt{s}$	$\int L\,dt$	data events	Monte Carlo events
205 GeV	83.0 pb^{-1}	411	443
206.5 GeV	137.6 pb^{-1}	710	708

Table 6.7: *Number of selected events for 2000 data compared to the number of selected events obtained from Monte Carlo studies.*

Again, the expected statistical errors obtained from Monte Carlo studies are included in parentheses.

$\sqrt{s}$	fitted mass	total error	stat. error	syst. error
205 GeV	80.590	0.197	0.190 (0.192)	0.053
206.5 GeV	80.543	0.158	0.149 (0.147)	0.054

Table 6.8: *Fit results for 2000 data and corresponding errors (in GeV). The values of the expected statistical errors are included in parentheses to allow comparison.*

The individual measurement results are combined using equation (6.17). A combination of both center-of-mass energies (205 and 206.5 GeV) yields the following result for the mass of the W boson in the semileptonic channel:

$$M_W = 80.562 \pm 0.117 \pm 0.050\,GeV$$

with a statistical error of 117 MeV and a systematic error of 50 MeV.

6.4.3 Combined Results

In the final step of this analysis, the results of all center-of-mass energies between 192 and 206.5 GeV are combined to yield one single value for the mass of the W boson. Again, a χ^2 function (equation 6.17) is minimized yielding the combined value. Correlations between systematic uncertainties are included in the covariance matrix (see chapter 6.1.4 for details). Correlated sources are uncertainties of the jet energy, the effects of Initial State Radiation, the hadronization model and the fit procedure. They are treated as fully correlated. Background and four-fermion effects, Monte Carlo statistics uncertainties and uncertainties in the lepton energy are treated as uncorrelated error sources [30].

A combination of all results included in this analysis yields the following value for the measured mass of the W boson in the semileptonic decay channel:

$$M_W = 80.575 \pm 0.079 \pm 0.051\,GeV$$

with a statistical error of 79 MeV and a systematic error of 51 MeV. These results prove to be in agreement with both the Standard Model expectations and results from other direct measurements of the mass of the W boson in the semileptonic channel. A detailed comparison with alternative results is given in the closing chapter.

Chapter 7

Discussion of Results

Now that the results are finally presented, the finishing chapter contains several alternatives in and to the fit routine used in this analysis. A short abstract about the use of the Blobel fit, an alternative constrained fit program implementing Lagrange multipliers in the event reconstruction, is given in the first part of this section. The Blobel fit was tested with a sample of Monte Carlo events but dropped in favour of a well tried method implementing penalty functions as it showed more stable results. In the following sections the results obtained from the convolution fit are compared to the results of alternative analysis methods yielding the mass of the W boson. The Breit-Wigner fit, a fit of an analytical Breit-Wigner function to a data sample, and its fit results are presented in 7.2.1 and compared with the convolution fit results in the same energy region. A comparison with combined LEP results of the measured W boson mass in the semileptonic channel is given in chapter 7.2.2. The section finally closes with a short summary of this thesis.

7.1 Comparison with an Alternative Reconstruction Method: The Blobel Fit

The convolution fit uses MINUIT [24], a CERN package designed to find the minimum value of a multi-parameter function, to minimize the χ^2 function and to perform the maximum likelihood fit. In doing so, the negative logarithm of the likelihood is minimized — a procedure equivalent to the maximisation of its positive logarithm — to allow the implementation of MINUIT.

During this analysis an attempt has been made to replace the MINUIT package by another fit routine designed for the minimisation of a multi-parameter function, the Blobel fit routine [26]. While this analysis employs MINUIT in combination with penalty functions in the kinematic fit to obtain the minimum value of the χ^2 function, the Blobel fit routine uses an iterative method implementing Lagrange multipliers for the minimisation (see [26] for details). Studies with different Monte Carlo samples show that the χ^2 functions of both methods yield consistent results. Examples for χ^2 functions obtained from a kinematic fit using MINUIT in combination with penalty functions and Blobel fit results are given in figure 7.1.

The Blobel fit yields fitted masses that are in good agreement with the corresponding MINUIT results. Both methods are applied to a Monte Carlo sample generated at a center-of-mass energy of $\sqrt{s} = 192\ GeV$. The resulting masses are plotted against each other in figure 7.2. As expected, the points are centered around the diagonal and accumulate at a mass value of about $80\,GeV$. To allow a more detailed comparison between the fitted masses, the difference between corresponding mass values, $m_{blobel} - m_{Minuit}$, is depicted as well. The distribution of $m_{blobel} - m_{Minuit}$ shows a distinct peak at $0\,GeV$. The results obtained from the Blobel fit can thus be seen as consistent with the results of a fit implementing MINUIT and penalty functions in the kinematic fit.

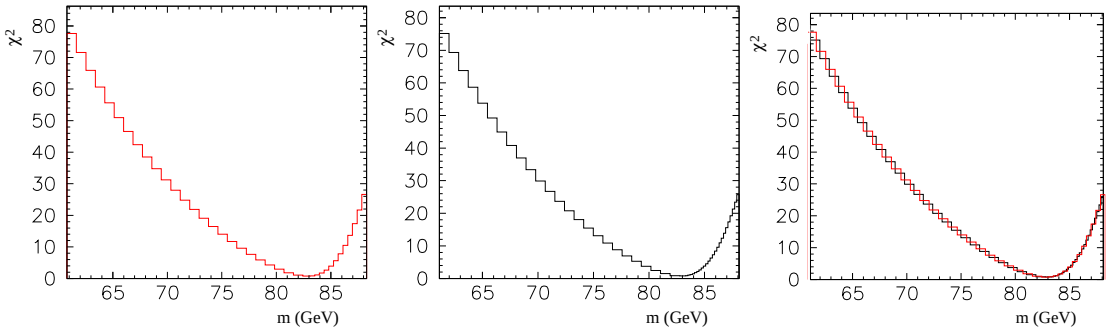

Figure 7.1: *Example of a χ^2 function obtained from a kinematic fit using the Blobel fit routine (left) and MINUIT in combination with penalty functions (in the middle). Both functions are plotted one over another in the third plot (right) to show that they are equivalent. The event depicted in this figure is taken from a Monte Carlo sample generated at a center-of-mass energy of $\sqrt{s}$=205 GeV.*

The great disadvantage that finally lead to the exclusion of the Blobel fit routine in this analysis is its relative instability compared to the use of MINUIT in combination with penalty functions in the kinematic fit. Studies on the subject show that the kinematic fit implementing MINUIT and penalty functions is decidedly more stable than the Blobel fit routine using Lagrange multipliers. The great advantage of the Blobel fit is its computational speed, reducing the processing time by a factor of about one over fifteen. A detailed account of both effect is given in table 7.1. Monte Carlo studies with 25000 events generated at a center-of-mass energy of $\sqrt{s} = 192\ GeV$ were made to obtain the results listed below.

As the fit procedure used in this analysis is not exceptionally time-consuming, the Blobel fit was dropped and the convolution fit was carried out using MINUIT in combination with penalty functions in the kinematic fit. The Blobel fit might prove useful in the 2-dimensional convolution fit, a method, where the masses of the two W bosons are varied separately. The 2-dimensional convolution method is far more time consuming than the 1-dimensional convolution fit employed in this analysis.

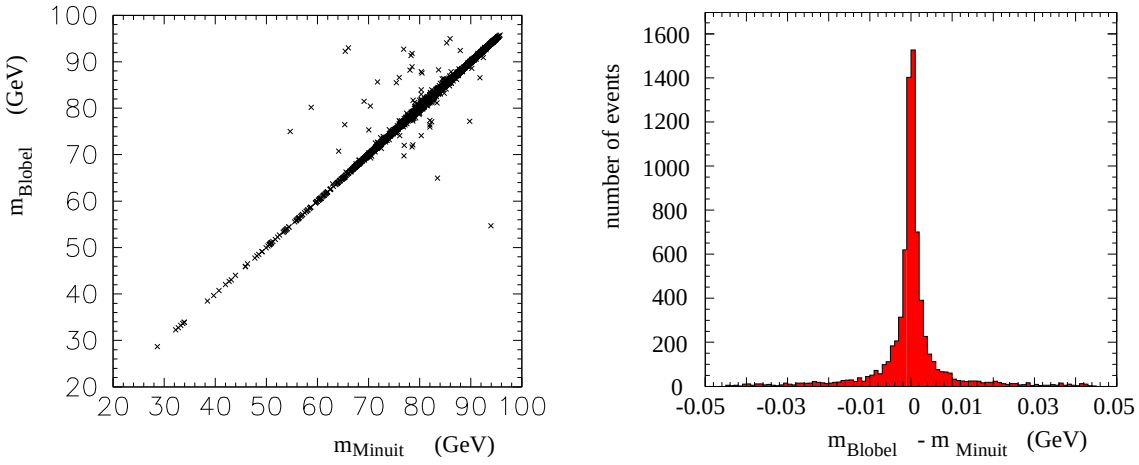

Figure 7.2: *Fitted masses obtained from a kinematic fit using the Blobel fit routine routine (y-axis) plotted against corresponding MINUIT results (x-axis) and the difference between corresponding mass values reconstructed with the Blobel fit routine and a kinematic fit using MINUIT for the minimisation of the χ^2 function. Monte Carlo events generated at a center-of-mass energy of $\sqrt{s} = 192\ GeV$ are used for this study.*

	N_{failed} / N_{total}	processing time
Blobel	$5.1 \cdot 10^{-2}$	35.71 s
MINUIT	$9.0 \cdot 10^{-3}$	529.72 s

Table 7.1: *Stability and speed differences between MINUIT and Blobel obtained from the computation of 25000 Monte Carlo events generated at a center-of-mass energy of $\sqrt{s} = 192\ GeV$. N_{failed} / N_{total} denotes the ratio of the number of events for which the fit failed to the total number of events.*

7.2 Comparison with Alternative Fit Results

7.2.1 Comparison with Results from the Breit-Wigner Fit

The Breit-Wigner fit is a conceptually more simple method used in the determination of the mass of the W boson. Like the convolution fit, it uses an unbinned maximum likelihood fit, in this case the fit of an analytic Breit-Wigner function, to a data sample. The effects of Initial State Radiation are considered by varying the widths in the peak region of the Breit-Wigner function. Monte Carlo simulations of the expected mass distribution yield these widths. In contrast to the convolution fit used in this analysis, the Breit-Wigner fit does not take the individual measurement errors of the different events into account. Both analysis methods use the same data events. It it thus justified to expect consistent results. But the correlations between the Breit-Wigner and the convolution fit results are reduced considerably by various effects such as the different fit procedure and the fact that the Breit-Wigner fit uses only a restricted energy region (masses between 70 and 88 GeV). The values for the W mass measurement obtained from the Breit-Wigner fit are therefore

well suited for a cross-check on the fit results of this analysis.

The Breit-Wigner fit results for 1999 data ($\sqrt{s}$ = 192–202 GeV) in the semileptonic channel are given below (table 7.2, see [31] for details) along with the results obtained from the convolution fit in the same energy region. Unfortunately the results for 2000 data are not yet available.

$\sqrt{s}$	Breit-Wigner fit	convolution fit
192 GeV	80.87 ± 0.29	80.86 ± 0.27
196 GeV	80.76 ± 0.18	80.88 ± 0.18
200 GeV	80.53 ± 0.19	80.34 ± 0.19
202 GeV	80.30 ± 0.27	80.16 ± 0.26

Table 7.2: *Results of the mass of the W boson (in GeV) in the semileptonic channel obtained from the Breit-Wigner fit and the convolution fit. The results are given with their statistical errors.*

A combination of the Breit-Wigner fit results of the mass of the W boson obtained from the analysis of 1999 data ($\sqrt{s}$=192–202 GeV) in the semileptonic channel is given below along with the convolution fit result of the same energy region and the corresponding statistical errors.

Breit-Wigner fit results: Convolution fit results:

$M_W = 80.622 \pm 0.109\,GeV$ $M_W = 80.581 \pm 0.108\,GeV$

A comparison between both results shows that the values of the mass of the W boson are consistent within the 1 sigma interval. The statistical error obtained from the convolution fit shows an improvement of 1 MeV. The convolution fit with its consideration of single event information thus leads to a slightly better resolution of the fit results for center-of-mass energies between 192 and 202 GeV.

7.2.2 Comparison with other LEP Results

The combination of all center-of-mass energies treated in this analysis yields — as already mentioned in 6.4.3 — a measured W boson mass of

$$M_W = 80.575 \pm 0.079 \pm 0.051\,GeV$$

The combined LEP results for the semileptonic channel and the contributions of all four experiments are depicted in figure 7.3. Data collected between 1996 and 2000 were used to obtain these results. The combined result of this analysis is consistent within the error ranges with a previous preliminary OPAL result and shows a deviation of about 1.2 σ from the combined preliminary result of all four LEP experiments.

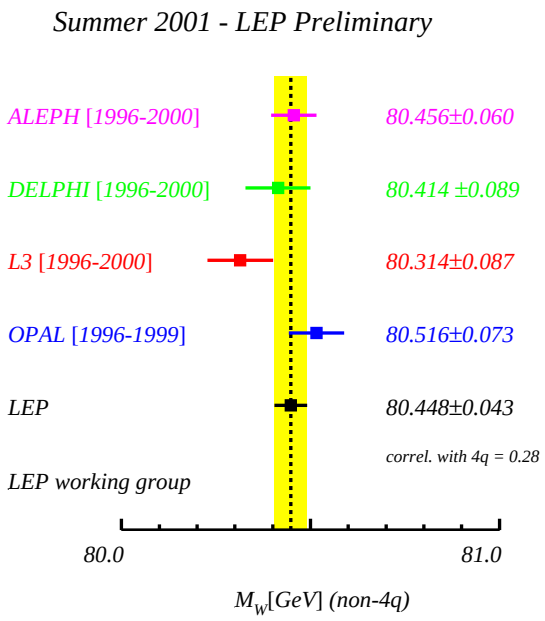

Figure 7.3: *Combined results of the measurement of the W boson mass in the semileptonic channel obtained from the analysis of data taken in the years 1996 to 2000. The solid line denotes the average value of the measured W boson mass of all four experiments. The corresponding measurement error is marked by the yellow band.*

7.3 Summary

The semileptonic decay channel is most important for the measurement of the mass of the W boson, as 44 percent of all W boson pairs decay semileptonically into a quark-antiquark and a lepton-neutrino pair. Only the statistics of the fully hadronic channel are comparable to the statistics of the semileptonic channel. But the impact of background processes is a lot smaller in the semileptonic channel, especially as there is no combinatorial background — the wrong association of jets to W bosons. Furthermore there are no effects of Final State Interaction — Bose-Einstein Correlations [8] and Colour Reconnection [9]. The semileptonic channel almost seems ideal to measure the mass of the W boson. But there is a disadvantage inherent in the semileptonic W boson pair decay. The lepton neutrino escapes undetected, carrying away an unknown amount of energy. The individual measurement errors therefore vary from event to event, the error distribution exceeds the natural width of the W boson Γ_W by far. A method that takes the individual errors of each event into account would be ideal for the determination of the W boson mass in the semileptonic decay channel. The convolution method meets this demand. The convolution fit is based on an unbinned likelihood fit, where a theoretical mass distribution is fitted to a data sample to obtain the mass of the W boson. An event probability density describing the probability, that a given event originated from a W boson of mass m, is convolved with a physics function representing the expected mass distribution to obtain the event likelihood. The total likelihood is given by the product of the individual event likelihoods.

A maximum likelihood fit finally yields the mass of the W boson. This method was applied to data collected at the OPAL detector in the years 1999 and 2000 including center-of-mass energies between 192 GeV and 206.5 GeV. A total of $437.6\,pb^{-1}$ of data was thus analysed, yielding the following combined result of the mass of the W boson:

$$\boxed{M_W = 80.575 \pm 0.079 \pm 0.051\,GeV}$$

The results of this analysis were compared to results obtained from a Breit-Wigner fit — the fit of an analytical Breit-Wigner signal function to a data sample — and found consistent with one another. The combined result for all 1999 and 2000 data in the semileptonic channel furthermore proved to be in good agreement with a preliminary OPAL result of the mass of the W boson.

Now that the 2000 data taking is finished, the days of LEP2 are also coming to an end. The OPAL detector, where the data analysed in this thesis was collected, is currently being dismantled. Like the measurement of the properties of the Z^0 boson being one of the great achievements of LEP1, the LEP2 era provided the means to measure the properties of W boson pairs. The W boson mass measurement can thus be considered as one of the major results of LEP2.

Bibliography

[1] Jörg Dubbert, Measurement of the W Boson Mass in the $W^+W^- \to \mathrm{q\bar{q}}l\bar{\nu}$ Channel with the OPAL Detector at LEP, München, November 2000

[2] Tim Christiansen, Influence of 5-Jet Events on the Measurement of the Mass of the W Boson in e^+e^- Collisions, diploma thesis, September 2000

[3] Peter Schmüser, Feynman-Graphen und Eichtheorien für Experimentalphysiker, Springer Verlag Berlin Heidelberg, 1995

[4] David Griffiths, Introduction to Elementary Particles, John Wiley and Sons, Inc., New York 1987

[5] The OPAL Collaboration, A Combination of Preliminary Electroweak Measurements and Constraints on the Standard Model, OPAL TN692, May 2001

[6] The OPAL Collaboration, Measurement of Standard Model Processes in e^+e^- Collisions at $\sqrt{s} > 202\,GeV$, November 2000

[7] W.J.Sterling, The Measurement of M_W from W^+W^- Threshold Cross Section at LEP2, DTP—95—24, February 1995

[8] The OPAL Collaboration, G. Abbiendi et al., Bose-Einstein Correlations in e+e- -¿ W+W- at 172 and 183 GeV, CERN-EP/98-174, October 1998

[9] O.Sahr, Colour Reconnection in hadronischen W-Paar Zerfällen, January 2001

[10] Monte Carlo program KORALW 1.02 for W-pair production at LEP2/NLC energies with Yennie-Frautschi-Suura exponentiation, CERN-TH/95-205, July 1995

[11] Torbjörn Sjöstrand, PYTHIA 5.7 and JETSET 7.4, Physics and Manual, December 1998

[12] J.Fujimoto, T.Ishikawa, K.Kato et altera, grc4f: a Four-fermion Event Generator for e^+e^- Collisions, May 96

[13] F.A. Berends and R. Pittau, R. Klein, All electroweak four fermion processes in electron-positron collisions, April 1994

[14] The Lund Monte Carlo Programs, CERN Pool programs W5035/W5045/ W5046/W5047/W5048 long writeup

[15] G.Corcella, I.G.Knowles, G.Marchesini, S.Moretti, K.Odagiri, P.Richardson, M.H.Seymour, B.R.Webber, Herwig 6: an event generator for Hadron Emission Reactions With Interfering Gluons, CERN-TH/2000-284

[16] Pat Ward, David Ward, A GOPAL Primer, January 1995

[17] R.Brun, GEANT3 Users Guide, Technical Report CERN/DD/84-1, CERN,1984

[18] S.L.Lloyd, The OPAL Primer, Version 97a, January 1997

[19] M.A. Thomson, The OPAL $W^+W^- \to \mathrm{q\bar{q}}l\bar{\nu}_l$ Event Selection, OPAL TN635, Cern, January 2000

[20] N.Brown, W.J.Sterling, Phys. Lett. B252 (1990) 657

[21] T.Omori, S.Asai, I.Nakamura and S.Yamashita, A Matching Algorithm: MT package, TN381, July 1996

[22] A.Frey, Subroutine WWEVLT

[23] C.Hartmann, Die Messung der Masse und Breite des W-Bosons und die Suche nach anomalen Drei-Boson-Kopplungen bei LEPII mit OPAL. Bonn, 1997

[24] F.James, MINUIT Reference Manual, Version 94.1, Cern, August 1998

[25] V.Blobel, E.Lohrmann, Statistische und numerische Methoden der Datenanalyse, Leipzig, 1998

[26] V.Blobel, Constrained Least Squares and Error Propagation, Hamburg, November 1997

[27] The LEP Energy Working Group, Evaluation of the LEP center-of-mass energy for data taken in 2000, March 2001

[28] D.Ward, draft on TN on updated WWFIX: WWFIX - fixups for the W mass analysis, June 2001

[29] The LEP Collaborations ALEPH, DELPHI, L3, OPAL, the LEP Electroweak Working Group and the SLD Heavy Flavour and Electroweak Groups, A Combination of Preliminary Electroweak Measurements and Constraints on the Standard Model, CERN-EP/2001-021, February 2001

[30] R.L.Coxe, Measurement of the Mass and the Width of the W Boson with the OPAL Detector, PhD thesis, University of Chicago, June 2000

[31] The OPAL Collaboration, Measurement of the Mass of the W Boson in e^+e^- annihilations at 192-202 GeV, OPAL PN422, July 2000

[32] web page: http://lepewwg.web.cern.ch/LEPEWWG/plots/summer2001/, July 2001

Appendix A

Monte Carlo Runs used in this Analysis

$\sqrt{s} = 192$ GeV	
Pythia $q\bar{q}$	5105
KoralW WW final states	
$M_W = 79.83$	9902
$M_W = 80.08$	9901
$M_W = 80.33$	9900
$M_W = 80.58$	9903
$M_W = 80.83$	9904
non-WW final states	9920
KoralW with Jetset	8755
KoralW with Herwig	8793
KoralW Single W	
$We\nu \to e\nu qq$	9880
$We\nu \to e\nu l\nu$	10503

$\sqrt{s} = 196$ GeV	
Pythia $q\bar{q}$	5106
KoralW WW final states	
$M_W = 79.83$	9907
$M_W = 80.08$	9906
$M_W = 80.33$	9905
$M_W = 80.58$	9908
$M_W = 80.83$	9909
non-WW final states	9921
KoralW with Jetset	9101
KoralW with Herwig	9124
KoralW Single W	
$We\nu \to e\nu qq$	9881
$We\nu \to e\nu l\nu$	10504

$\sqrt{s} = 200$ GeV	
Pythia $q\bar{q}$	5121
KoralW WW final states	
$M_W = 79.83$	9912
$M_W = 80.08$	9911
$M_W = 80.33$	9910
$M_W = 80.58$	9913
$M_W = 80.83$	9914
non-WW final states	9922
KoralW with Jetset	9540
KoralW with Herwig	9541
KoralW Single W	
$We\nu \to e\nu qq$	9882
$We\nu \to e\nu l\nu$	10505

$\sqrt{s} = 202$ GeV	
Pythia $q\bar{q}$	5126
KoralW WW final states	
$M_W = 79.83$	9917
$M_W = 80.08$	9916
$M_W = 80.33$	9915
$M_W = 80.58$	9918
$M_W = 80.83$	9919
non-WW final states	9923
KoralW with Jetset	9726
KoralW with Herwig	9727
KoralW Single W	
$We\nu \to e\nu qq$	9883
$We\nu \to e\nu l\nu$	10506

$\sqrt{s}$ = 205 GeV	
Pythia $q\bar{q}$	5183
KoralW WW final states	
$M_W = 79.83$	11398
$M_W = 80.08$	11399
$M_W = 80.33$	11400
$M_W = 80.58$	11401
$M_W = 80.83$	11402
non-WW final states	10404
KoralW with Jetset	10324
KoralW with Herwig	10325
KoralW Single W	
$We\nu \to e\nu qq$	10189
$We\nu \to e\nu l\nu$	10188

$\sqrt{s}$ = 206.5 GeV	
Pythia $q\bar{q}$	5190
KoralW WW final states	
$M_W = 79.83$	11408
$M_W = 80.08$	11409
$M_W = 80.33$	11410
$M_W = 80.58$	11411
$M_W = 80.83$	11412
non-WW final states	11414
KoralW with Jetset	10324
KoralW with Herwig	10325
KoralW Single W	
$We\nu \to e\nu qq$	10189
$We\nu \to e\nu l\nu$	10188

Appendix B

W Boson Mass in the different Decay Channels

Results for the mass of the W boson and statistical errors in GeV.
The expected statistical errors are included in parentheses for matters of comparison.

	1999 data	2000 data	1999 and 2000 data combined
$q\bar{q}e\bar{\nu}_e$	80.602 ± 0.165 (0.177)	80.820 ± 0.177 (0.189)	80.704 ± 0.121 (0.129)
$q\bar{q}\mu\bar{\nu}_\mu$	80.702 ± 0.183 (0.183)	80.358 ± 0.199 (0.195)	80.545 ± 0.135 (0.133)
$q\bar{q}\tau\bar{\nu}_\tau$	80.343 ± 0.224 (0.220)	80.358 ± 0.253 (0.244)	80.350 ± 0.168 (0.163)
$q\bar{q}l\bar{\nu}_l$	80.581 ± 0.108 (0.110)	80.562 ± 0.117 (0.119)	80.575 ± 0.079 (0.081)

Appendix C

Systematic Errors in the different Decay Channels

	$\sqrt{s} = 192\,GeV$		
	$q\bar{q}e\bar{\nu}_e$	$q\bar{q}\mu\bar{\nu}_\mu$	$q\bar{q}\tau\bar{\nu}_\tau$
beam energy	17	14	17
bias correction	19	56	30
Initial State Radiation	1	1	1
jet energy	2	3	7
lepton energy	17	20	1
hadronization	40	42	46
background	35	32	39
four-fermion effects	2	0	1
fit procedure	1	1	1

	$\sqrt{s} = 196\,GeV$		
	$q\bar{q}e\bar{\nu}_e$	$q\bar{q}\mu\bar{\nu}_\mu$	$q\bar{q}\tau\bar{\nu}_\tau$
beam energy	15	15	18
bias correction	35	28	21
Initial State Radiation	1	1	1
jet energy	2	3	7
lepton energy	18	23	1
hadronization	65	38	59
background	33	36	48
four-fermion effects	2	0	1
fit procedure	1	1	1

	$\sqrt{s} = 200\,GeV$		
	$q\bar{q}e\bar{\nu}_e$	$q\bar{q}\mu\bar{\nu}_\mu$	$q\bar{q}\tau\bar{\nu}_\tau$
beam energy	16	15	16
bias correction	27	21	41
Initial State Radiation	1	1	1
jet energy	2	4	3
lepton energy	24	25	2
hadronization	42	52	59
background	39	39	34
four-fermion effects	2	0	1
fit procedure	1	1	1

	$\sqrt{s} = 202\,GeV$		
	$q\bar{q}e\bar{\nu}_e$	$q\bar{q}\mu\bar{\nu}_\mu$	$q\bar{q}\tau\bar{\nu}_\tau$
beam energy	13	16	18
bias correction	23	27	22
Initial State Radiation	1	1	2
jet energy	2	2	7
lepton energy	21	28	1
hadronization	59	49	77
background	36	43	49
four-fermion effects	2	0	1
fit procedure	1	1	1

	$\sqrt{s} = 205\,GeV$		
	$q\bar{q}e\bar{\nu}_e$	$q\bar{q}\mu\bar{\nu}_\mu$	$q\bar{q}\tau\bar{\nu}_\tau$
beam energy	15	16	19
bias correction	26	17	31
Initial State Radiation	1	2	2
jet energy	2	3	7
lepton energy	23	26	1
hadronization	41	37	62
background	15	42	45
four-fermion effects	2	0	1
fit procedure	1	1	1

	$\sqrt{s} = 206.5\,GeV$		
	$q\bar{q}e\bar{\nu}_e$	$q\bar{q}\mu\bar{\nu}_\mu$	$q\bar{q}\tau\bar{\nu}_\tau$
beam energy	17	16	19
bias correction	23	19	20
Initial State Radiation	1	1	2
jet energy	2	2	6
lepton energy	24	25	1
hadronization	38	36	49
background	42	45	46
four-fermion effects	2	0	1
fit procedure	1	1	1

Acknowledgement

At this point I would like to thank a number of people without whom this thesis would never have come into existence:
First of all Prof. Dorothee Schaile for waking my interest in particle physics in her lecture and for giving me the possibility to do my thesis in this field of research.
My tutors Jörg Dubbert and Fritz Vollmer for their help and support and for answering all my questions.
Günter Duckeck and the other members of the OPAL W group for new ideas and discussions about my analysis.
Otto Schaile for rescuing me from a number of emergencies whenever my computer went down in the summer heat.
The other members of the Garching group, especially Michael Bussmann, for creating an open and friendly atmosphere that made work a lot easier.
Herta Franz for having solutions to all major and minor problems associated with the creation of a diploma thesis.
And last but not least Peter and my parents for being there for me whenever things did not turn out as planned.

Ich versichere hiermit, die vorliegende Arbeit selbständig verfasst zu haben und keine anderen als die angegebenen Quellen und Hilfsmittel benutzt zu haben.

München, 2.August 2001

Birgit Bußmann